Decanuclear Ln_{10} Wheels and Vertex-shared Spirocyclic Ln_5 Cores: Synthesis, Structure, SMM Behavior and MCE Properties

Sourav Das[a], Atanu Dey[a], Subrata Kundu[a], Sourav Biswas[a], Ramakirushnan Suriya Narayanan[c], Silvia Titos-Padilla[b], G. Lorusso[d], M. Evangelisti[d], Enrique Colacio*[b] and Vadapalli Chandrasekhar*[a, c]

[a] Department of Chemistry, Indian Institute of Technology Kanpur, Kanpur-208016, India;

Homepage: http://www.iitk.ac.in

[b] Departamento de Química Inorgánica, Facultad de Ciencias, Universidad de Granada, Avenida de Fuentenueva s/n, 18071 Granada, Spain

Homepage: http://www.ugr.es

[c] National Institute of Science Education and Research, Institute of Physics Campus, Sachivalaya Marg, PO: Sainik School, Bhubaneswar - 751 005, India;

Homepage: http://www.niser.ac.in

[d] Instituto de Ciencia de Materiales de Aragón and Departamento de Física de la Materia Condensada, CSIC-Universidad de Zaragoza, 50009 Zaragoza, Spain

Abstract

The reaction of a Schiff-base ligand (LH_3) with lanthanide salts, pivalic acid and triethylamine in 1:1:1:3 and 4:5:8:20 stoichiometric ratios results in the formation of decanuclear Ln_{10} [Ln= Dy(**1**), Tb(**2**) and Gd(**3**)] and pentanuclear Ln_5 complexes [Ln= Gd(**4**), Tb(**5**) and Dy(**6**)] respectively. The formation of Ln_{10} and Ln_5 complexes are fully governed by the stoichiometry of the reagents used. Detailed magnetic studies on these complexes (**1**-**6**) have been carried out. Complex **1** shows a SMM behavior with an effective energy barrier for the reversal of the magnetization (U_{eff}) = 16.12(8) K and relaxation time (τ_o) = 3.3 x 10^{-5} s under 4000 Oe *dc* field. Complex **6** shows the frequency dependent maxima in the out-of-phase signal under zero *dc* field, without achieving maxima above 2K. Complexes **3** and **4** show a large magnetocaloric effect with the following characteristic values: $-\Delta S_m$ = 26.6 J kg^{-1} K^{-1} at T = 2.2 K for **3** and $-\Delta S_m$ = 27.1 J kg^{-1} K^{-1} at T = 2.4 K for **4**, both for an applied field change of 7 T.

Key words: Decanuclear and pentanuclear lanthanide complexes, single-molecule magnetism, magnetocaloric effect.

Introduction

Polynuclear lanthanide complexes have caught the imagination of chemists and physicists in recent years for a variety of reasons.[1] Discovering new synthetic methods that allow the modulation of the nuclearity and topology of such complexes is an endeavor that is being pursued vigorously by chemists while the magnetic properties of such complexes (single-molecule magnetism[2] and magneto caloric effect[3]) are of interest to the chemists and physicists alike. In this context, polynuclear lanthanide complexes where the nuclearity is 5 or 10 are quite sparse. Our interest in such systems has emanated from our recent forays in this field where we have been able, by utilizing hydrazone Schiff-base ligands, to assemble tetra-,[4a],[4b] hexa-[4c] and octanuclear[4d] complexes. The latter possessed a novel cyclooctadiene-type of conformation.[4d] We were interested to extend the nuclearity of the macrocycle through a judicious choice of a suitable multidentate ligand. Caneschi, *et al*. has previously reported a Dy_{10} macrocycle using methoxy ethanol as the ligand but only measured its static magnetism.[5a] Since then, other examples, though sparse, are becoming known. Similar to decanuclear complexes,[5] pentanuclear[6] analogues are equally rare; in fact only four previous families are known. It is worth noting that some cyclic Dy_3[7], Dy_4[8] and Dy_6[9] complexes have been shown to exhibit a toroidal magnetic moment in the ground state, which is due to the non-collinear arrangement of the local magnetic moments of the individual Dy^{III} centers. Moreover, most of these systems present SMM behaviour which is associated with the thermally excited spin states of the Dy_n molecule. These systems also called Single-molecule Toroics (SMTs) are promising candidates for future applications in quantum computing and information storage. It should be mention that the linkage of two and even more cyclic Dy_3 SMTs give rise to coupled systems where the

toroidal ground sate is robust as the easy axial anisotropy axes are very difficult to be modified by the interaction between the coupled units[10]

Herein, we report a new chelating, flexible and sterically unencumbered multisite coordinating ligand (*E*)-2-((2-hydroxyethylimino)methyl)-6-(hydroxymethyl)-4-methylphenol (LH_3) which allows the assembly of both deca- and pentanuclear lanthanide complexes. Most interestingly, both these new families of polynuclear lanthanide complexes do not contain oxide/hydroxide ligands which are commonly found in many such complexes. Accordingly, herein, we report the synthesis, structural characterization and magnetic studies of $[Ln_{10}(LH)_{10}(\kappa^2\text{-Piv})_{10}]\cdot XCHCl_3\cdot YCH_3CN\cdot PH_2O\cdot QMeOH$ (**1**, Ln = Dy(III), X = 9, Y = 4; **2**, Ln = Tb(III), X = 8, Y = 4; **3**, Ln = Gd(III), X = 8, Y = 3, P = 5;) and $[Ln_5(LH)_4(\mu_2\text{-}\eta^1\eta^1\text{Piv})_4(\eta^1\text{Piv})(S)]\cdot XH_2O\cdot YCH_3OH$ (**4**, Ln = Gd(III),S = MeOH, X = 3, Y = 1; **5**, Ln = Tb(III), S = H_2O, X = 3, Y = 2; **6,** Ln = Dy(III), S = MeOH, X = 2, Y = 1). While **1**-**3** are metallamacrocycles, **4**-**6** possess a pentanuclear core constructed by two Ln_3 triangles sharing a common lanthanide ion.

Results and Discussion

Synthesis

Recently we have been experimenting with various types of ligands for the purpose of knowing their discriminatory capability in terms of directing homonuclear lanthanide assemblies vs heteronuclear 3d/4f complexes.[11] Thus, the ligands, 2-(hydroxymethyl)-6-carbaldehyde-4-methylphenol (**C2**) and the Schiff base derivative (2-(2-hydroxy-3-(hydroxymethyl)-5-methylbenzylideneamino)-2-methylpropane1,3-diol) afforded pentanuclear M_4Ln[11a],[11b] and M_2Ln[11c], [11d], [11e] derivatives respectively (Scheme 1).

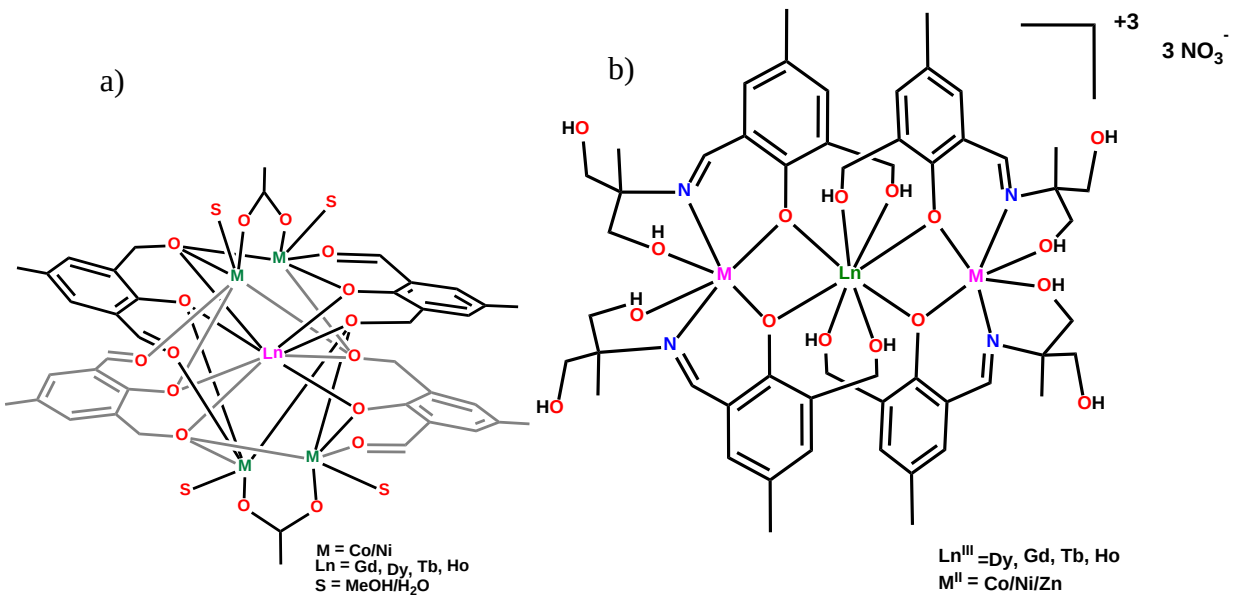

Scheme 1. a) Pentanuclear M_4Ln[11a], [11b] and b) trinuclear M_2Ln[11c],[11d][11e] derived from **C2** and its Schiff base derivative respectively.

Neither of these ligands, however, was able to assemble homonuclear lanthanide complexes. We reasoned that while **C2** does not possess enough flexible coordinating pockets, while its Schiff base derivative 2-(2-hydroxy-3-(hydroxymethyl)-5-methylbenzylideneamino)-2-methylpropane1,3-diol (Scheme 1b), has two -CH_2OH arms fused to the same carbon centre making it a rigid system. Such rigid ligands are generally not suitable for polynuclear lanthanide complex assembly. To overcome these drawbacks we have designed a new chelating, flexible, and sterically unencumbered multisite coordinating compartmental Schiff-base ligand (*E*)-2-((2-hydroxyethylimino)methyl)-6-(hydroxymethyl)-4-methylphenol (LH_3). The ligand LH_3 was prepared by a two-step synthetic protocol involving the conversion of the precursor **C1** to **C2** and its subsequent condensation with 2-amino ethanol (Scheme 2).

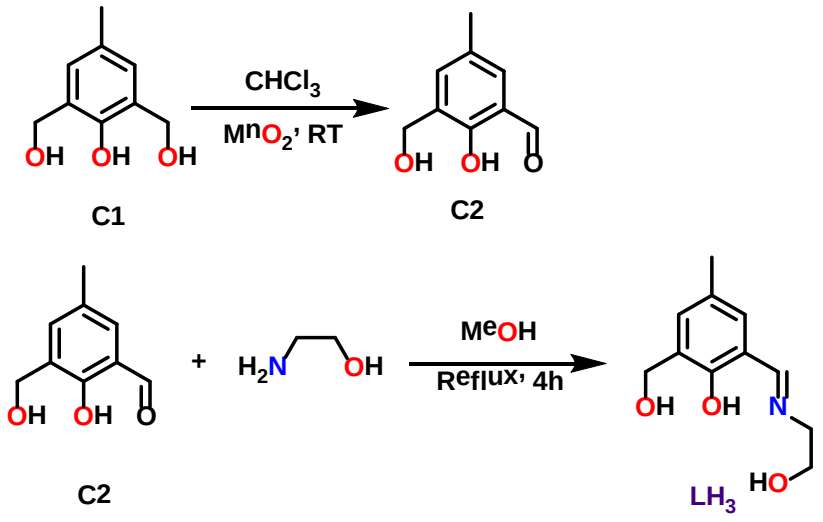

Scheme 2. Synthesis of LH_3

LH_3 contains two coordination compartments; one of these possesses a phenolic oxygen and a benzyl oxygen atom (chelating OO donor). The other compartment consists of a phenolic oxygen and a flexible ethanolamine group (tridentate ONO donor) (Scheme 3).

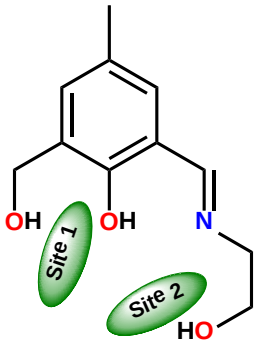

Scheme 3. The two distinct coordination compartments of LH_3. Site 1 contains a chelating OO coordination manifold while Site 2 provides ONO cavity.

Thus, potentially LH_3 contains four divergent coordinating centers all of which are anticipated to participate in coordination to construct a homometallic ensemble. Also, we are aware that the -

CH_2OH unit can bind both in its native and de-protonated forms, in the latter it can act as a bridging ligand and enable formation of larger polynuclear complexes. In this synthesis we also utilized pivalic as a co-ligand because of the propensity of the pivalate ion to bridge adjacent metal centers.[12],[4b],[4d] The reaction of LH_3 with Ln(III) salts along with pivalic acid in the presence of triethylamine under two different conditions afforded deca-(**1-3**) and pentanuclear complexes (**4-6**) (Scheme 4).

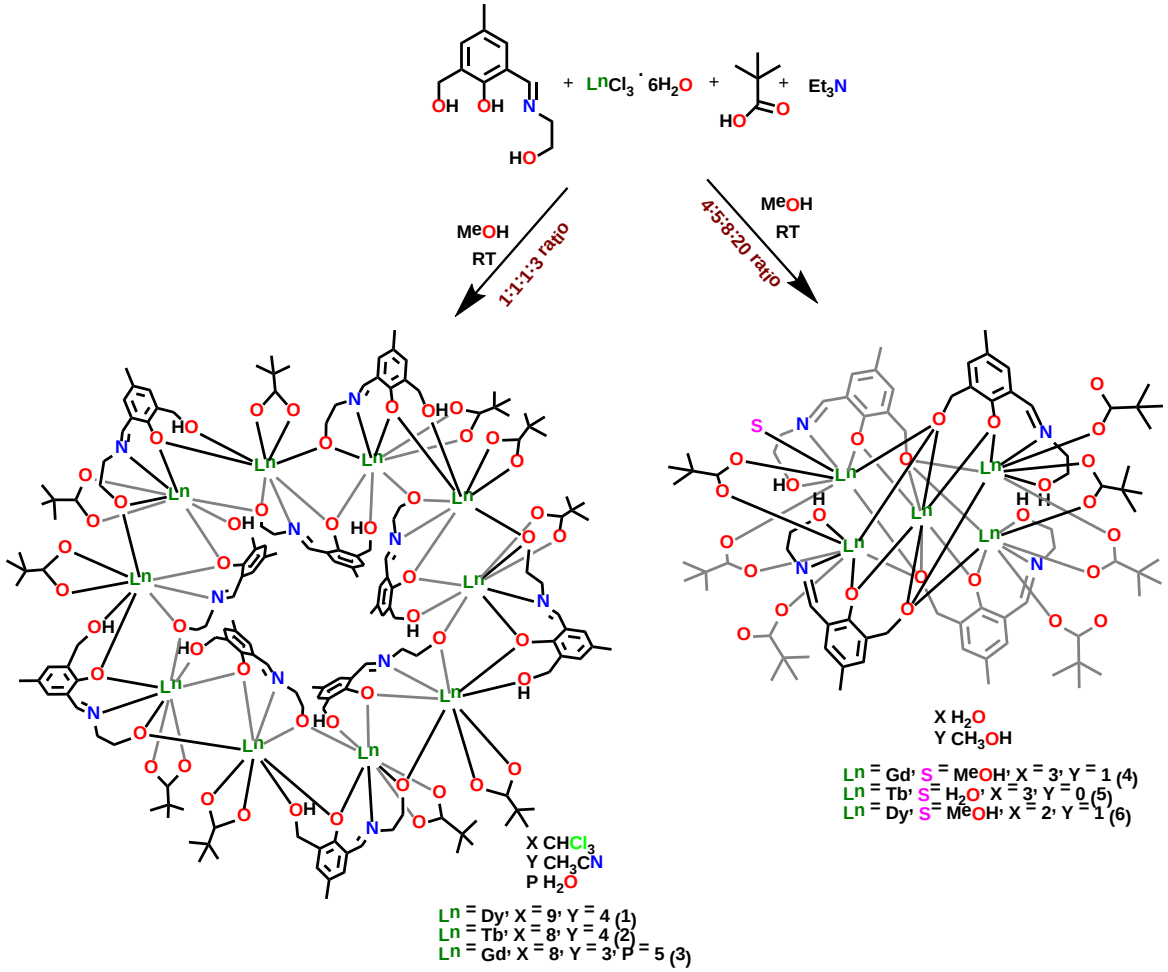

Scheme 4. Synthesis of the homometallic Ln_{10} macrocyclic complexes **1-3** where the deprotonated oxygen atom of ethanolamine acts as a bridging group in LH_3 (left side); synthesis

of the homometallic Ln_5 complexes where the deprotonated benzylic oxygen atom acts as capping μ_3-O unit (right side).

Subtle variation in stochiometry, including that of the base triethylamine causes interesting de-protonation behavior. Thus, in the decanuclear complexes, **1-3**, the $=N\text{-}CH_2CH_2OH$ is deprotonated while the $\text{-}CH_2OH$ arm is not. In the case of the pentanuclear complexes the situation is reversed. The molecular structures of **1-6** were delineated by their single-crystal diffraction studies as outlined below.

X-ray Crystal Structures of 1-3

Single crystal X-ray analysis reveals that **1-3** crystallize in the triclinic system in the centrosymmetric *P*-1 space group with Z = 2. The asymmetric unit of **1-3** consists of two half molecules viz., $[Ln_5(LH)_5(Piv)_5]$ where Ln= Dy(**1**), Tb(**2**) and Gd(**3**). Because of the structural similarity of **1-3**, only the structure of **1** is described, here, in detail. The others are given in the Supporting Information.

The molecular structure of **1** is given in Figure 1; those of **2** and **3** are given in the Supporting Information (Figures S1-S2). Selected bond parameters of **1** are summarized in the Table 1. Other bond parameters including those of **2-3** are given in the Supporting Information (Tables S1-S2).

The crystal structure of **1** (Figure 1a) reveals it to be a macrocycle that is assembled as a result of the cumulative coordination action of 10 $[LH]^{2-}$ ligands each of which binds in a μ_3 - η^2: η^1: η^2: η^1 fashion (Scheme 5). In addition to $[LH]^{2-}$, ten pivalate ions participate in coordination each of which being involved in binding to only one Dy(III) ion. Most interestingly, **1** does not contain any other common ligands such as oxide or hydroxide, which are generally found in polynuclear lanthanide complexes.

An analysis of the molecular structure of **1**, reveals that the macrocylce contains interconnected Dy_2O_2 four-membered rings possessing spirocyclic Dy(III) nodes. The macrocycle itself is 20-membered, considering the shortest Dy-O-Dy pathway. The Dy(III) ions organize themselves in the complex in a *chair-chair-chair* conformation (Figure 1b).

a)

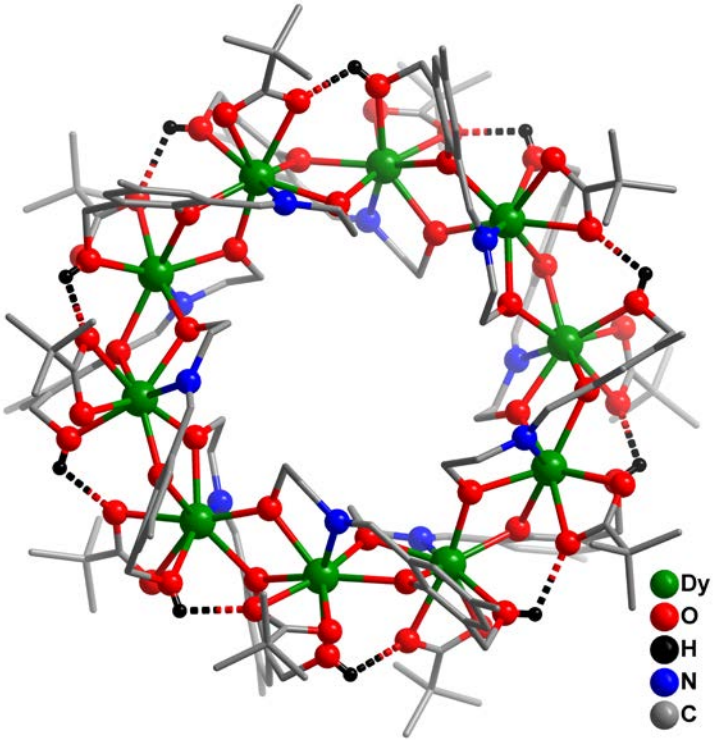

b)

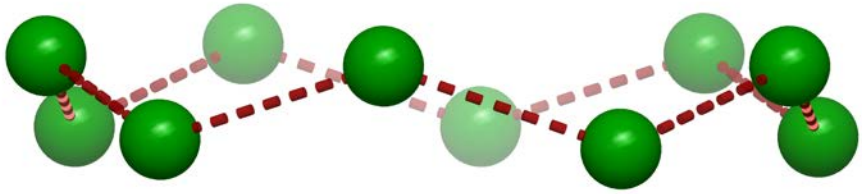

Figure 1. (a) Molecular structure of **1** (hydrogen atoms and the solvent molecules have been omitted for clarity). (b) The Dy_{10} metallacycle possessing a chair-chair-chair conformation.

Table 1. Selected bond distance (Å) and bond angle (°) parameters for **1** are as follows:

Dy(1P)-O(13P)*	2.237(4)	Dy(2P)-O(18P)	2.474(4)	Dy(5P)-O(14P)	2.376(4)
Dy(1P)-O(1P)	2.294(4)	Dy(3P)-O(4P)	2.237(4)	Dy(5P)-O(3P)	2.414(4)
Dy(1P)-O(2P)	2.386(4)	Dy(3P)-O(7P)	2.300(4)	Dy(5P)-O(2P)*	2.420(4)
Dy(1P)-O(6P)	2.402(4)	Dy(3P)-O(8P)	2.363(4)	Dy(5P)-N(5P)	2.455(5)
Dy(1P)-O(5P)	2.438(4)	Dy(3P)-O(12P)	2.395(4)	Dy(5P)-O(24P)	2.462(4)
Dy(1P)-O(17P)	2.454(4)	Dy(3P)-O(11P)	2.431(4)	Dy(5P)-O(25P)	2.467(4)
Dy(1P)-O(16P)	2.459(4)	Dy(3P)-N(3P)	2.447(5)	Dy(4P)-C(71P)	2.849(6)
Dy(1P)-N(1P)	2.466(5)	Dy(3P)-O(21P)	2.462(4)	Dy(5P)-O(10P)	2.242(4)
Dy(1P)-Dy(5P)*	3.8107(4)	Dy(3P)-O(20P)	2.498(4)	Dy(5P)-O(13P)	2.304(4)
Dy(2P)-O(1P)	2.247(4)	Dy(4P)-O(7P)	2.232(4)	Dy(2P)-O(1P)-Dy(1P)	114.61(17)
Dy(2P)-O(4P)	2.303(4)	Dy(4P)-O(10P)	2.303(4)	Dy(1P)-O(2P)-Dy(5P)*	104.91(15)
Dy(2P)-O(5P)	2.356(4)	Dy(4P)-O(11P)	2.371(4)	Dy(3P)-O(4P)-Dy(2P)	113.53(16)
Dy(2P)-O(9P)	2.397(4)	Dy(4P)-O(15P)	2.380(4)	Dy(2P)-O(5P)-Dy(1P)	105.70(15)
Dy(2P)-O(8P)	2.424(4)	Dy(4P)-O(14P)	2.418(4)	Dy(4P)-O(7P)-Dy(3P)	114.85(19)
Dy(2P)-O(19P)	2.438(5)	Dy(4P)-O(23P)	2.447(4)	Dy(3P)-O(8P)-Dy(2P)	104.97(14)
Dy(2P)-N(2P)	2.468(5)	Dy(4P)-N(4P)	2.464(5)	Dy(5P)-O(10P)-Dy(4P)	114.63(16)
		Dy(4P)-O(22P)	2.508(4)	Dy(4P)-O(11P)-Dy(3P)	105.33(15)
				Dy(1P)*-O(13P)-Dy(5P)	114.10(16)
				Dy(5P)-O(14P)-Dy(4P)	105.85(14)

Symmetry transformations used to generate equivalent atoms: *1 -x+1,-y+1,-z+1

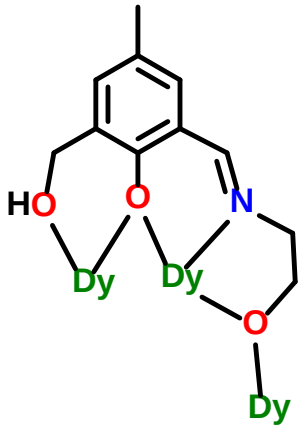

μ_3 - η^2: η^1: η^2: η^1

Scheme 5. Binding mode of the ligand $[LH]^{2-}$ with Dy^{III} ions.

The assembly of the macrocyle **1** is accomplished in the following manner. The four-membered non-planar Dy_2O_2 ring is built by the coordination action of bridging phenolate and $=NCH_2CH_2O^-$ that emanate from two different ligands. The inter-Dy(III) distances and the Dy–O–Dy angles in the four-membered rings are in the range 3.797-3.831 Å and 105.60 (2)–114.85(1)° respectively. All the Dy(III) centers are eight-coordinate (7O, 1N) and possess a distorted-triangular dodecahedral geometry (Figure 2b).

a)

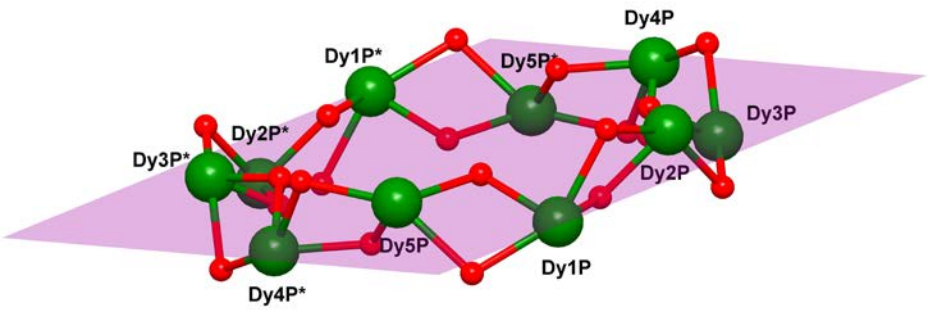

b)

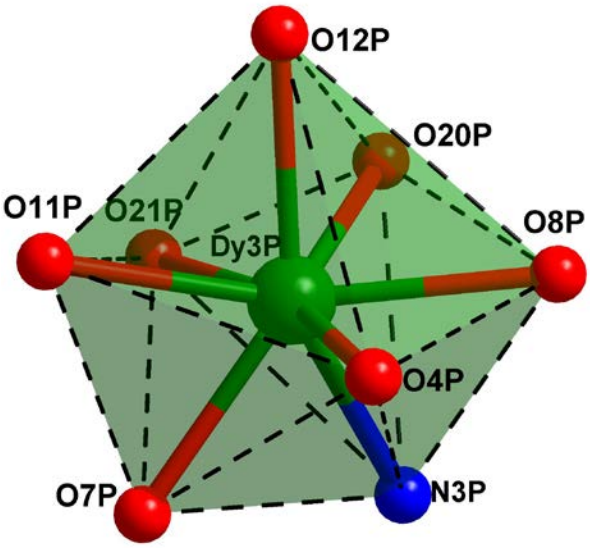

Figure 2. (a) 20-membered macrocycilc core with a meanplane. (b) A distorted-triangular dodecahedral geometry around Dy(III) ion.

A few further comments on the molecular structure of **1**. With respect to the mean plane (considering all the Dy atoms) of the macrocycle, alternate Dy atoms lie above and below (average 0.578 (7) Å) the plane (Figure 2a). Interestingly, each LH^{2-} alternately is placed above and below the plane of the Dy_{10} wheel. Complex **1** displays strong intramolecular O–H···O (2.187 (6) Å) hydrogen-bonding interactions between the pivalic carboxylate oxygen atoms and the Dy coordinated benzyl alcohol (-CH_2OH) arms (Figure 1a). The supramolecular structure of **1** reveals a 2D-architecture within which is found a chloroform channel, where the trapped cholorofom molecules are stabilized by hydrogen bonding interactions (Figures S3 and S4). An idea about the macrocyclic ring size of **1** can be obtained from the distances between the symmetry equivalent Dy atoms, which are in the range 11.696 (6) to 11.976 (7) Å.

In spite of the large interest in 4*f*-complexes, it is surprising to note that only a few Ln_{10} complexes are known in literature. As mentioned earlier Caneschi and coworkers in 2003 first reported a Dy_{10} wheel containing methoxyethanol as a bridging ligand.[5a] The molecular topology of **1** is similar to this literature precedent although the ligands used are entirely different. Another example of decanuclear complexes {Ln_{10}} (Ln = Dy or Gd) reveals that nine Dy^{III} metal ions are present in a ring while a tenth Dy^{III} metal ion is located at the centre of the structure.[5b] Finally, another Dy_{10} ensemble is known containing vertex-fused Dy_3 triangles[5c] (Figure 3).

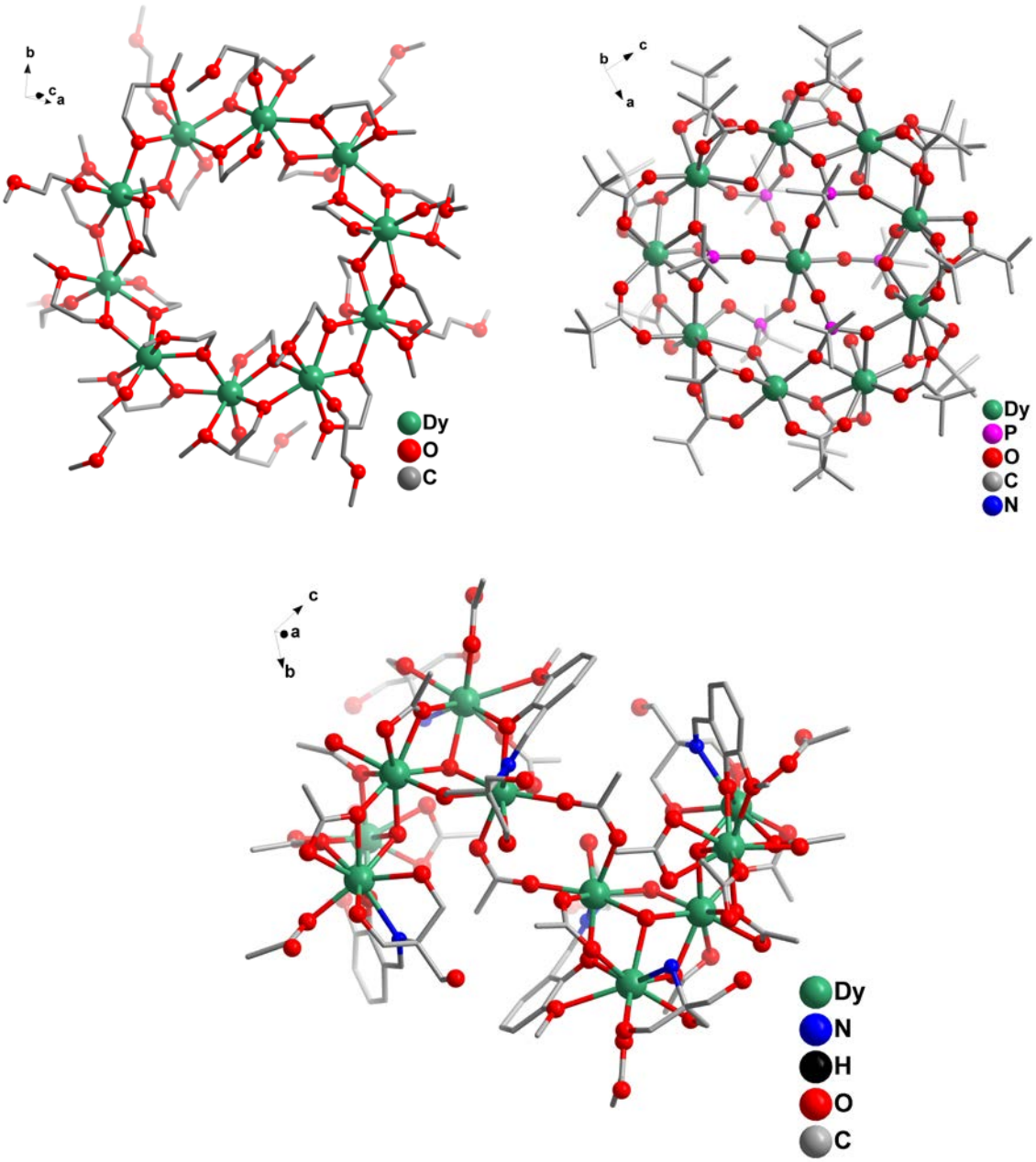

Figure 3. Examples of reported discrete decanuclear lanthanide complexes.

X-ray Crystal Structures of 4-6

X-ray crystallographic analysis of **4-6** reveals that all these complexes crystallize in the monoclinic system in the $P2_1$ chiral space group with Z = 2. Compounds **4-6** are neutral and

possess a nearly similar structural arrangement with only minor structural variations (Scheme 4 and Supporting Information). The asymmetric unit of **4**-**6** consists of a full molecule $[Ln_5(LH)_4(\mu_2\text{-}\eta^1\eta^1Piv)_4(\eta^1Piv)(MeOH/H_2O)]$. The refined Flack parameters of **4**-**6** are 0.010(13), -0.003(10) and 0.013(11) respectively indicating the crystallization of enantiopure forms.

In view of their structural similarity, we describe, herein, the molecular structure of **6** as a representative example; the structural details of **4**-**5** are given in the Supporting Information (Figures S5 and S6). A perspective view of the molecular structure of **6** is depicted in Figure 4. The caption of Figure 4 and Figure 5a summarizes the selected bond parameters of **6**. The molecular structures and selected bond parameters of the other two compounds (**4** and **5**) are given in the Supporting Information (Figures S5-S6, Tables S3-S4).

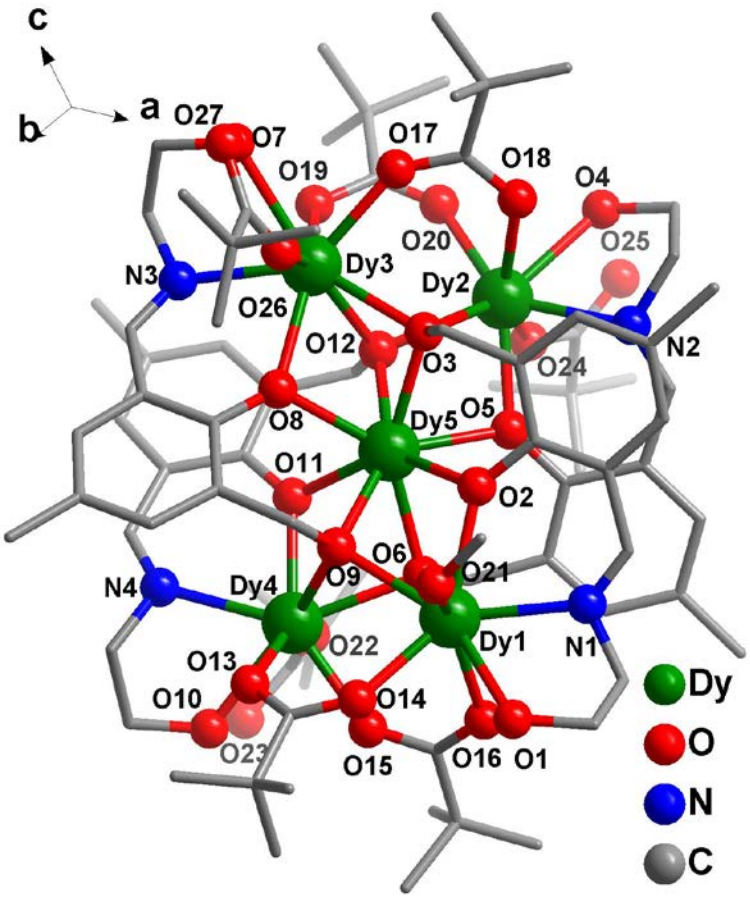

Figure 4. Molecular structure of **6** (hydrogen atoms and the solvent molecules have been omitted for clarity). Selected bond distance (Å) and bond angle (°) parameters are as follows: Dy(1)-O(2) = 2.343(7); Dy(1)-O(6) = 2.382(7); Dy(1)-O(9) = 2.396(7); Dy(1)-N(1) = 2.452(10); Dy(1)-O(1) = 2.516(8); Dy(2)-O(5) =2.317(6); Dy(2)-O(12) =2.404(6); Dy(2)-N(2) = 2.433(8); Dy(2)-O(3) = 2.460(7); Dy(2)-O(4) = 2.513(8); Dy(3)-O(8) = 2.367(6); Dy(3)-O(3) = 2.425(6); Dy(3)-N(3) = 2.437(8); Dy(3)-O(12) =2.456(6); Dy(3)-O(7) =2.535(7); Dy(4)-O(11) = 2.327(7); Dy(4)-O(6) = 2.445(7); Dy(4)-N(4) = 2.451(9); Dy(4)-O(9) = 2.460(7); Dy(4)-O(10) =2.474(8); Dy(5)-O(3) = 2.300(6); Dy(5)-O(9) = 2.302(7); Dy(5)-O(12) = 2.313(6); Dy(5)-O(6) = 2.330(6); Dy(5)-O(5) = 2.366(6); Dy(5)-O(11) = 2.368(6); Dy(5)-O(8) = 2.377(6); Dy(5)-O(2) = 2.399(7); Dy(5)-O(3)-Dy(3) = 97.06(2); Dy(3)-O(3)-Dy(2) = 97.07(2); Dy(5)-O(3)-Dy(2) = 96.16(2); Dy(2)-O(5)-Dy(5) = 98.33(2); Dy(5)-O(6)-Dy(1) = 97.41(2); Dy(5)-O(6)-Dy(4) = 95.79(2); Dy(1)-O(6)-Dy(4) = 98.17(3); Dy(3)-O(8)-Dy(5) = 96.53(2); Dy(5)-O(9)-Dy(1) = 97.74(3); Dy(5)-O(9)-Dy(4) =96.10(3); Dy(1)-O(9)-Dy(4) = 97.32(2); Dy(4)-O(11)-Dy(5) = 98.02(2); Dy(5)-O(12)-Dy(2) =97.28(2); Dy(5)-O(12)-Dy(3) = 95.74(2); Dy(2)-O(12)-Dy(3) = 97.66(2)

The molecular structure of **6** reveals that the five Dy(III) ions are held together by four doubly deprotonated $[LH]^{2-}$ heptadentate Schiff-base ligands. Each such ligand holds four different Dy(III) ions in a μ_4-η^3:η^2:η^1:η^1 fashion (Scheme 6).

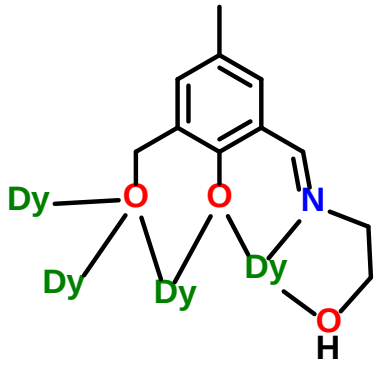

μ_4 - η^3: η^2: η^1: η^1

Scheme 6. Binding mode of the ligand $[LH]^{2-}$ with Dysprosium(III) ions.

Each ligand provides one benzyl alcoholic μ_3-oxygen atom, one phenolic μ_2-oxygen and one unidentate flexible chelating ethanolamine group (bidentate NO donor) (Scheme 6). Further analysis of the structure of **7** reveals some interesting features. Thus, **7** contains a pentanuclear $[Dy_5(\mu_3\text{-}O)_4(\mu_2\text{-}O)_4]^{+7}$ core consisting of triangular motifs $[Dy_3(\mu_3\text{-}O)_2(\mu_2\text{-}O)_2]^{+5}$ that are fused with each other through a common vertex (Dy5) (Figure 5). Each triangular unit is capped by two μ_3-O deprotonated benzyl alcohol oxygen atoms derived from two separate ligands. The μ_2-O phenolate oxygen atoms bridge the edges of the triangles. In addition to the binding provided by LH^{2-}, the peripheral Dy(III) ions are further held together as a result of two μ_2-η^1:η^1 binding action of the pivalate anions. Finally, in order to satisfy the charge and coordination requirements, other pivalate anions coordinate the terminal Dy(III) ions in a monodentate fashion.

As mentioned above the pentanuclear Dy_5 core consists of two interconnected Dy_3 motifs. The dihedral angle between these two is 60.78(2)°. Also, the central dysprosium ion (Dy5) is part of six Dy_2O_2 four-membered rings (Figure 5b).

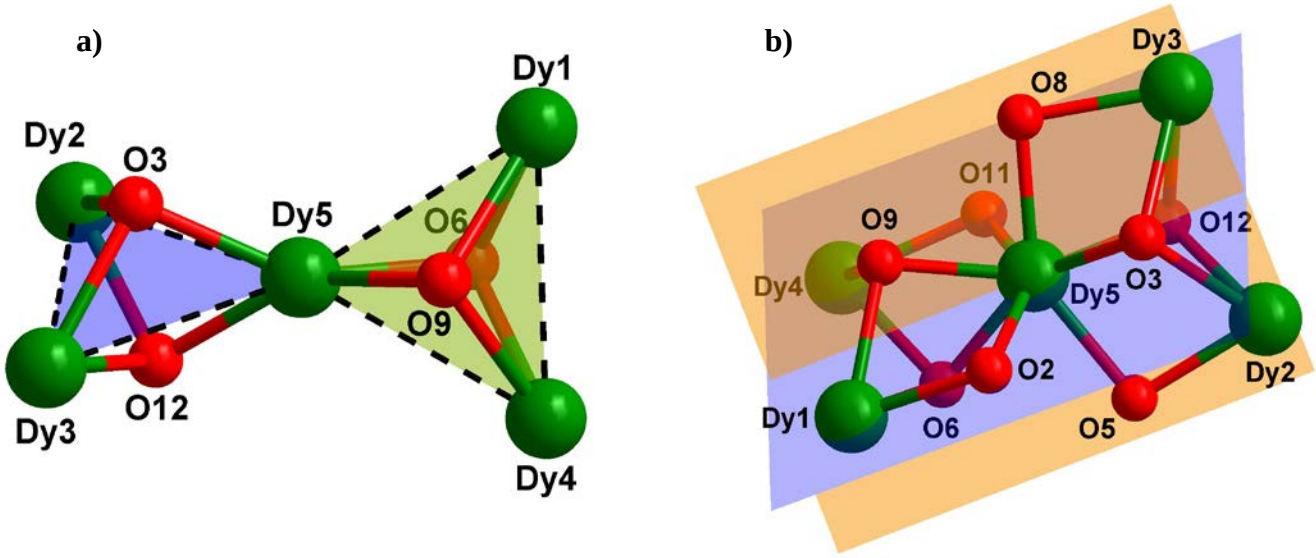

Figure 5. (a) Vertex-fused triangular unit capped by two μ_3-O alkoxy group from above or below face of the triangle. Intermetallic distances (Å) and angles (°): Dy2-Dy3 = 3.658(12); Dy2-Dy5 = 3.541(9); Dy3-Dy5 = 3.540(12); Dy5-Dy4 = 3.542(9); Dy1-Dy4 = 3.648(8); Dy5-Dy1 = 3.539(13); Dy2-Dy3-Dy5 = 58.91(1); Dy5-Dy2-Dy3 = 62.21(2); Dy3-Dy2-Dy5 = 58.87(1); Dy5-Dy4-Dy1 = 58.94(1); Dy4-Dy5-Dy1 = 60.02(2); Dy5-Dy1-Dy4 = 59.09(2). (b) Non planar disposition of the vertex fused triangular unit.

Finally, the central Dy(III) in **7** is eight coordinated in an *all-oxygen* coordination environment and in a distorted-triangular dodecahedral geometry (Figure 6a). In contrast, the peripheral Dy(III) ions, although also eight-coordinate possess a different coordination environment (7O,1N) and -geometry (distorted square antiprism geometry) (Figure 6b).

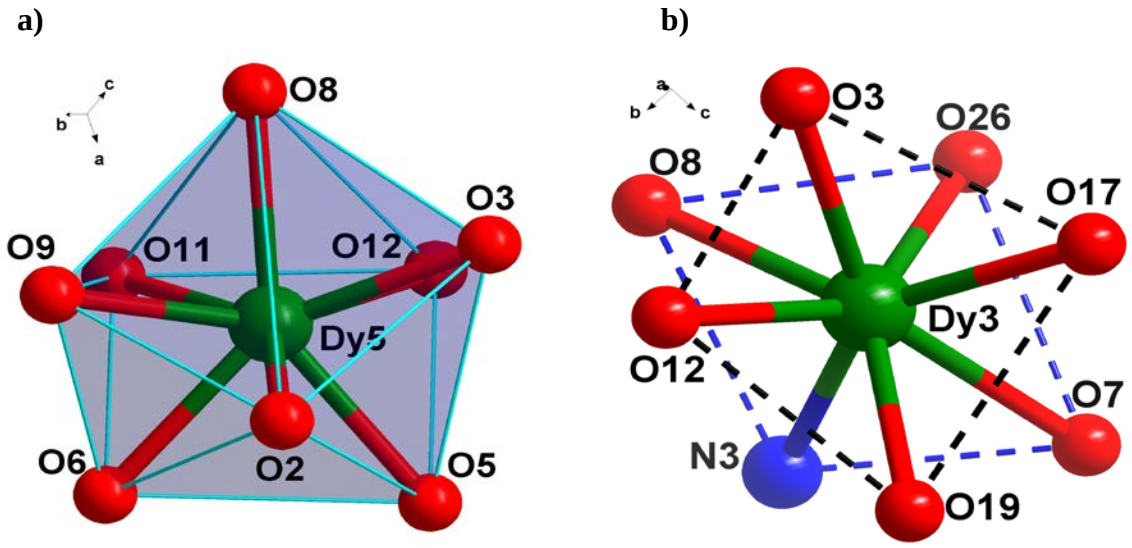

Figure 6. Different geometries around octa-coordinated Dy(III) ions (a) distorted-triangular dodecahedral (b) distorted square-antiprism geometry.

Interestingly, again, it is surprising to note that only a handful of Ln_5 complexes[6] are known in the literature whose magnetic behavior has been well-studied. Some of these are summarized in Figure 6 revealing that three structural types are thus far known viz. square-pyramidal[6a-c], trigonal bipyramidal[6d] and butter fly-shaped[6e]. The current family, thus represents a new structural type among pentanuclear Ln_5 complexes. Again, similar to the decanuclear complexes, the pentanuclear complexes reported herein do not contain O^{2-}/OH^- ligands.

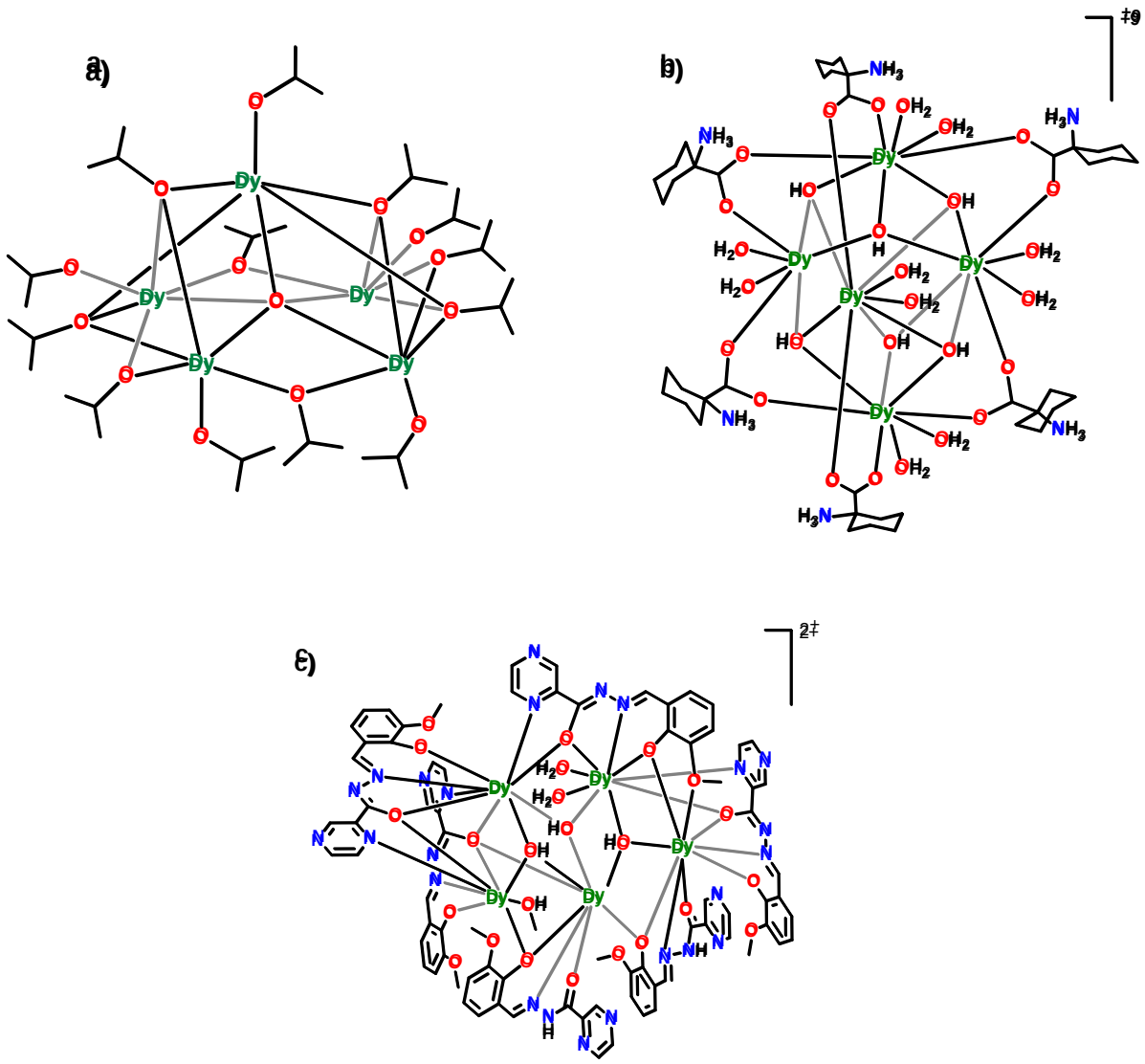

Figure 6. Examples of reported discrete pentanuclear lanthanide complexes [6] having a) square pyramidal b) trigonal bipyramidal and c) butterfly core.

Magnetothermal Properties

The temperature dependence of $\chi_M T$ for complexes **1-6** (χ_M is the molar magnetic susceptibility per Ln_n unit) in the range 300-2 K were measured in an applied magnetic field of 0.1 T (Figure 7).

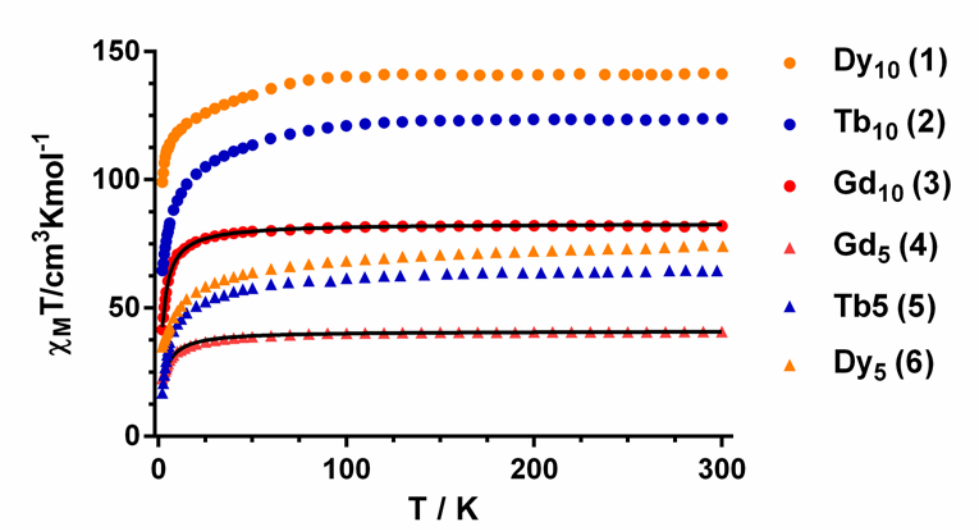

Figure 7. Temperature dependence of the $\chi_M T$ product for complexes **1-6**. The black solid lines show the best fits for complexes **3** and **4**.

The room temperature $\chi_M T$ values for complexes **1-6** are close to those calculated for isolated Ln^{III} ions in the free-ion approximation (Table 2).

Table 2. Direct current magnetic data for **1-6**.

Compound	Spin-orbit Ground state of the Ln^{3+} ion	$\chi_M T$ theoretical[a]/ at 300 K / at 2K (cm^3Kmol^{-1})	Calculated saturation vaue [b] / M at 2 K and 5 T ($N\mu_B$)
1	$^6H_{15/2}$, g_J =4/3	141.7/141.30/99.19	100/55.54
6	$^6H_{15/2}$, g_J =4/3	70.85/74.17/34.99	50/30.59

3	$^8S_{7/2,}$ g_J =2	78.75/82.12/41.56	35/34.40
4	$^8S_{7/2,}$ g_J =2	39.375/40.77/22.67	70.0/70.64
2	$^7F_6$, g_J =3/2	118.2/123.80/64.64	90/50.12
5	$^7F_6$, g_J =3/2	59.10/64.65/17.09	45/27.43

[a] Calculated with $\chi_M T = \frac{N\beta^2}{3k}\{g_j^2 J(J+1)\}$

[b] Calculated with $M = Ng_J J\mu_B;\ J = L + S\ ;\ g_J = \frac{3}{2} + \frac{S_T(S_T+1) - L(L+1)}{2J(J+1)}$

We start with the simpler cases concerning the Gd complexes **3** and **4**. On cooling, the $\chi_M T$ product for **3** and **4** remains almost constant until ~ 75 K and 100 K, respectively, and then decreases sharply down to 2 K. Since Gd^{3+} ions present no first order spin-orbit coupling, the decrease of the $\chi_M T$ product at low temperature is mainly due to the presence of a very weak antiferromagnetic interaction between the Gd^{3+} ions and/or ZFS effects of the ground state. This is supported by the field dependence of the magnetization at 2 K for **3** and **4**, which are well below the Brillouin function for ten and five non-interacting Gd^{3+} ions, respectively (Figure 8). At high field the saturation of the magnetization is almost complete at 5 T, reaching values that agree well with the theoretical saturation values for ten and five Gd^{3+} ions, respectively.

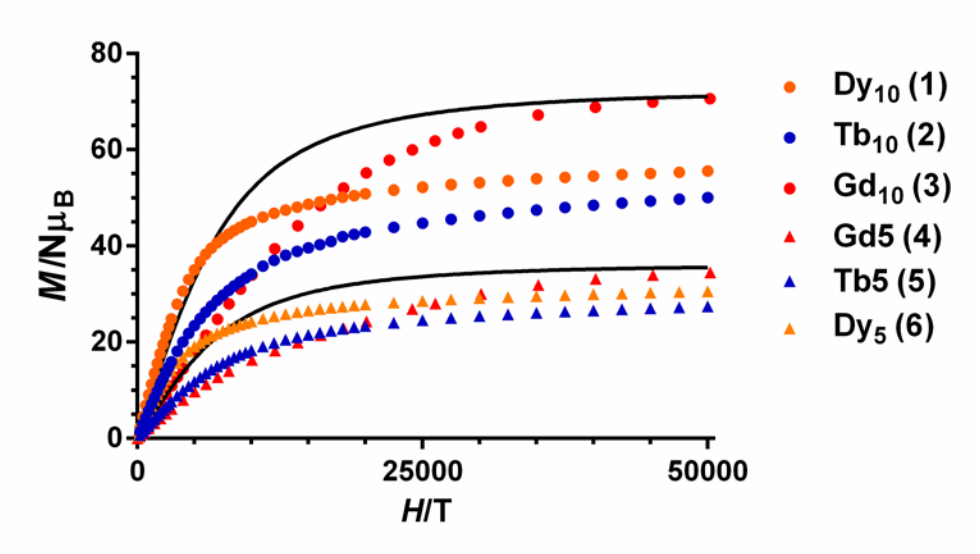

Figure 8. Field dependence of the magnetization for complexes **1**-**6** at 2K. The black solid lines represent the Brillouin function for non-interacting Gd^{3+} ions.

The magnitude of the antiferromagnetic exchange interaction in **3** could not be determined by diagonalization matrix methods because of the extremely high dimension of the matrices to be diagonalized for a Gd_{10} system. Nevertheless, in order to estimate the value of the magnetic exchange coupling mediated by the μ-alkoxido/μ-phenoxido pathway in **3** we have used a very crude model, in which each wheel has been considered to be formed by ten mononuclear Gd units and the intermononuclear interactions calculated by using the molecular field theory. Taking into account the above considerations, the experimental data were analyzed with the following Hamiltonian:

$$\hat{H} = zJ' < S_z > \hat{S}_z + g_i \beta H \sum_i \hat{S}_i$$

The best fitting parameters were zJ' = -0.0127(1) cm^{-1} and g = 2.054(1). Although the obtained values are similar to the reported coupling constants for dialkoxo and diphenoxo-bridged Gd^{3+} complexes, with or without carboxylate bridges connecting the Gd^{3+} ions,[13] they should be

taken with caution because: (i) the crudeness of the model and (ii) the possible existence of ZFS splitting of the Gd^{3+} ions.

As indicated above, compound **4** exhibits a structure that consists of two vertex fused triangles with two different types of bridging units between the Gd^{3+} ions: (i) di-μ_3-dialkoxido/μ-phenoxido, linking the central Gd^{3+} ion to the outer counterparts with Gd-Gd distances of approximately 3.540 Å and (ii) di-μ_3-dialkoxido /di-μ-syn-syn pivalato connecting each couple of outer Gd^{3+} ions with Gd-Gd distances of approximately 3.650 Å. Although the Gd-Gd distances slightly differ between the two fused triangles, to analyze the magnetic properties the four Gd-Gd distances corresponding to the type (i) bridging fragments were considered to be all equal. Likewise, the two outer type (ii) distances were considered to be equal. Taking into account the above considerations, the magnetic properties of **4** were modelled using the following two-*J* isotropic Hamiltonian:

$$\hat{H} = -J_1(\hat{S}_{Gd1}\hat{S}_{Gd5} + \hat{S}_{Gd2}\hat{S}_{Gd5} + \hat{S}_{Gd3}\hat{S}_{Gd5} + \hat{S}_{Gd4}\hat{S}_{Gd5}) - J_2(\hat{S}_{Gd1}\hat{S}_{Gd4} + \hat{S}_{Gd2}\hat{S}_{Gd3})$$

where J_1 and J_2 describe the magnetic exchange pathways involving short and long Gd···Gd distances, respectively (Figure 9).

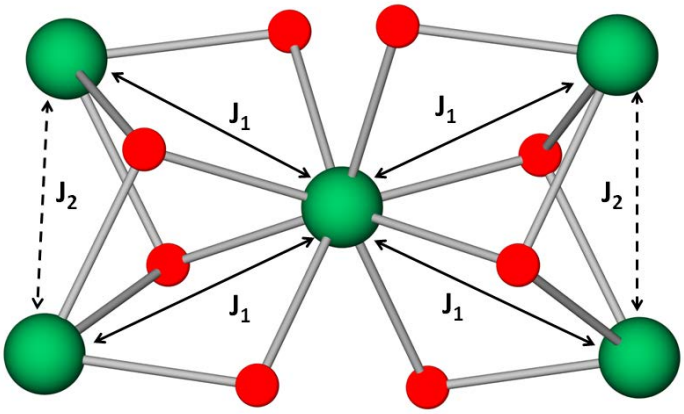

Figure 9. Coupling scheme for complex **4**.

The D_{Gd} is assumed to be negligible as this ion is rather isotropic. The simultaneous fit of the experimental magnetization and susceptibility data with the above Hamiltonian using the PHI program[14] afforded the following set of parameters: J_1 = -0.15 cm^{-1}, J_2 = -0.072 cm^{-1} and g = 2.04 with R = 5 x 10^{-5} ($R = \Sigma(\chi_{obs}T\ \chi_{calc}T)^2/\Sigma(\chi_{obs}T)^2$) where χ_{calc} and χ_{obs} denote calculated and observed molar magnetic susceptibilities, respectively. As in the case of compound **3**, the obtained values are in good agreement with the reported coupling constants for dialkoxo and diphenoxo-bridged Gd^{3+} complexes, with or without carboxylate bridges connecting the Gd^{3+} ions.[13] The structural differences between the Gd_2O_2 bridging fragments involving short and long Gd···Gd distances could be responsible for the different magnetic coupling of the two magnetic pathways. In this regard, theoretical and experimental studies carried out on oxygen-bridged Gd_2 complexes (alkoxido, phenoxido and carboxylate) complexes have suggested that J becomes more negative as the Gd-O-Gd, and consequently the Gd···Gd, decrease.[13a,f] The extracted J values for **3** and **4** agree well with this hypothesis as the former, that has larger Gd-O-Gd angles and Gd-Gd distances, exhibits the weaker Gd-Gd magnetic exchange interactions. In **4**, the shorter di-μ_3-dialkoxido/μ-phenoxido magnetic exchange pathway, linking the central and

outer Gd^{3+} ions exhibits the stronger magnetic exchange coupling, whereas the long di-μ_3-dialkoxido/di-μ-syn-syn pivalato pathway shows a much weaker magnetic coupling, as expected. Nevertheless, more examples of well magneto-structural characterized oxygen-bridged Gd_n complexes are needed to confirm the above assumption.

We have studied the magnetothermal properties of **3** and **4** because: (i) the magnetic interactions between the Gd^{3+} ions are relatively weak for both compounds; (ii) the Gd^{3+} ion shows negligible anisotropy due to the absence of orbital contribution; (iii) the Gd^{3+} exhibits the largest single-ion spin (S_{Gd} = 7/2) arising from the $4f^7$ electron configuration. These characteristics are known to favour a large MCE,[3a] i.e., the change of the magnetic entropy (ΔS_m) following a change of the applied field. The entropy changes that characterize **3** and **4** can be calculated straightforwardly from the experimental heat capacity, *C*, (Figure S7) after obtaining the entropy according to the expression:

$$S(T,B) = \int_0^T \frac{C(T,B)}{T} dT$$

Likewise, ΔS_m can also be calculated from the magnetization data (Figure S8) by making use of the Maxwell relation:

$$\Delta S_m = (T, \Delta B) = \int_{B_i}^{B_f} \left[\frac{\partial M(T,B)}{dT} \right]_B dB$$

where B_i and B_f are the initial and final applied magnetic fields. Figure xx shows the dependence of $-\Delta S_m$ on temperature and applied field changes, for both compounds. Note the nice agreement between the results obtained via both methods, thus validating the approaches employed. For the largest applied field change ΔB = 7 T, the maximum value of $-\Delta S_m$ is 26.6 J kg^{-1} K^{-1} at T = 2.2 K

for **3** and 27.1 J kg^{-1} K^{-1} at T = 2.4 K for **4**. Under our experimental conditions, the weak though not negligible antiferromagnetic interactions between the Gd^{3+} ions inhibit $-\Delta S_m(T,\Delta B)$ to attain the maximum entropy value per mole involved, i.e., $nR\ln(2S_{Gd} + 1) = 20.8\ R = 29.7$ J kg^{-1} K^{-1} for **3** and $10.4\ R = 35.4$ J kg^{-1} K^{-1} for **4**. Finally, the so-obtained $-\Delta S_m$ values for ΔB = 7 T are similar to those found for other Gd_5 and Gd_{10} complexes, but lower than those found for other magnetically-denser Gd_n polynuclear complexes.[15] The results for **3** and **4** suggest that these systems can be a good approach for molecular magnetic refrigerants.

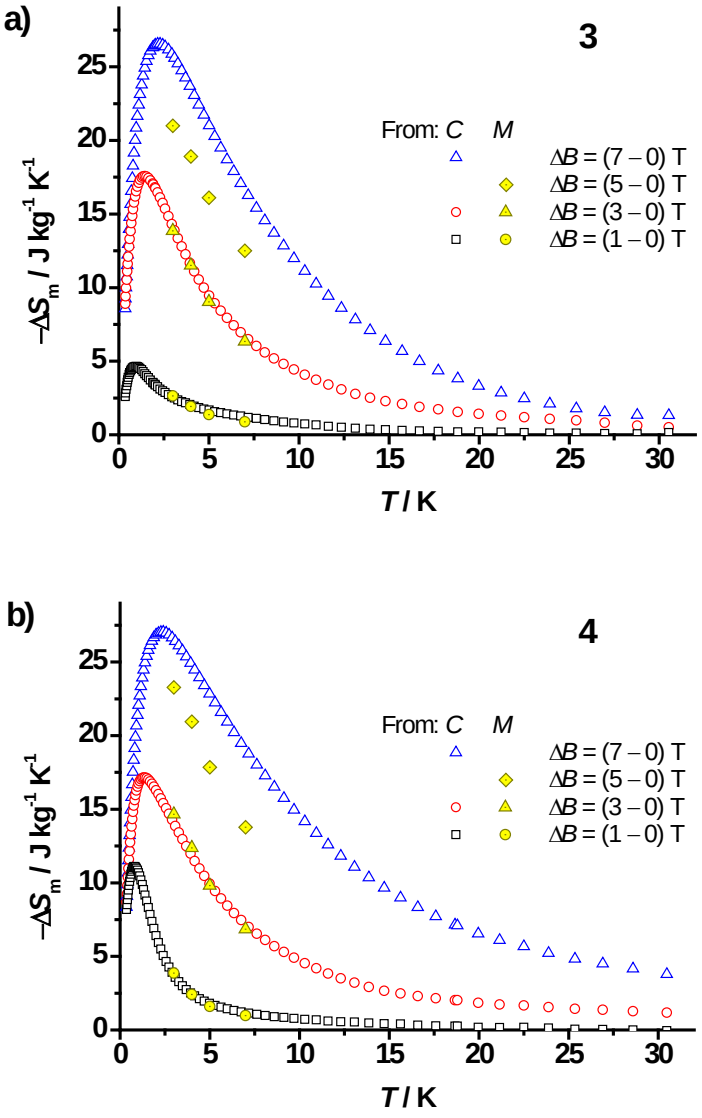

Figure 10. The dependence of the magnetic entropy change on temperature and selected applied field changes, for **3** (a) and **4** (b), as obtained from heat capacity and magnetization data.

As for the Dy^{3+} (**1** and **6)** and Tb^{3+} (**2** and **5)** complexes, the $\chi_M T$ product steadily decreases down to 2 K, which is due to the depopulation of the excited m_j sublevels of the Dy^{3+} and Tb^{3+} ions. This behavior which arises from the splitting of the $^6H_{15/2}$ and $^7F_6$ ground terms,

respectively, by the ligand field, and/or possible very weak intermolecular interactions between the Ln^{3+} ions.

The field dependence of the magnetization for the Dy^{3+} and Tb^{3+} complexes are given in Figure 8. The *M* versus *H* plot at 2 K for these complexes shows a relatively rapid increase in the magnetization at low field to reach almost the saturation for magnetic fields of 5T. The observed values at 5T are rather lower than expected, which is due to crystal-field effects leading to significant magnetic anisotropy.[16]

Dy^{3+} complexes are good candidates to exhibit SMM behavior because: (i) Dy^{3+} is a Kramers ion and therefore the ground state bistability is guaranteed (ii) it has a large moment $^6H_{15/2}$ spin orbit ground component and (iii) the *f* electronic cloud is largely anisotropic with an oblate shape, which can be stabilized by an axial crystal field that minimize the repulsive interactions between the ligands and *f*-electrons charge cloud.[17] Since the axial ligand field can be easily attained by serendipity in low symmetry Dy^{3+} complexes, easy–axis anisotropy of the ground state and consequently SMM behavior is often observed for these complexes. In view of the above considerations, the low symmetry DyO_7N and DyO_8 coordination environments observed for **1** and **6** could lead to SMM behavior. In order to know if compounds containing Dy^{3+} (**1** and **6)** and Tb^{3+} (**2** and **5)** exhibit slow relaxation of the magnetization and SMM behavior, *ac* magnetic susceptibility measurements as a function of the temperature and frequency were performed under zero and with small applied magnetic *dc* fields. The results of these measurements demonstrate that only compound **6** exhibit frequency dependence the out-of-phase (χ''_M) signals under zero *dc* field and therefore slow relaxation and probably SMM behavior (Figure 11).

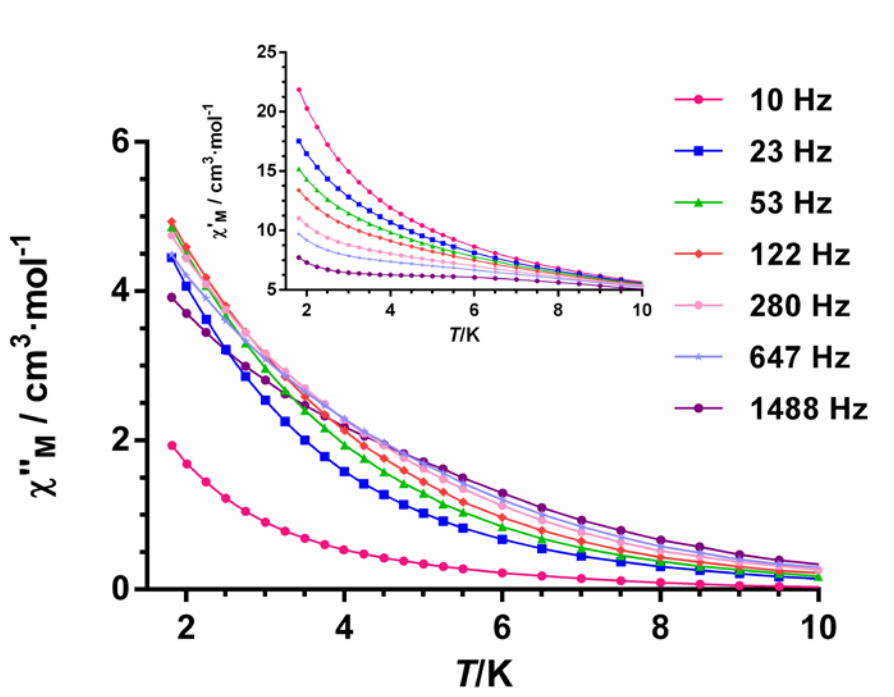

Figure 11. In-phase (χ'_M) and out-of-phase (χ''_M) signals under zero *dc* fields for **6**.

However, no maxima are observed in the temperature dependence of χ''_M above 2 K at frequencies reaching 1500 Hz, which does not allow to extract the value of the thermal activated energy barrier for the relaxation of the magnetization. When the *ac* measurements were performed in the presence of a small external *dc* field in the range 1000-4000 Oe, to fully or partly suppress the possible fast quantum tunneling relaxation, the temperature dependence of χ''_M for **6** did not significantly change with field. However, compound **1** shows a clear frequency dependence the out-of-phase (χ''_M) signals below ~10K under a H_{dc} = 2000 Oe, typical of thermally activated relaxation process (Figure S9). The χ''_M signals are broad with maxima in the 6.75 K(1488 Hz)-5.22 K (280 Hz) range and a tail below ~4 K (χ''_M does not go to zero below the maxima but increases up to 2 K). This can be attributed to overlapping of different relaxation processes, including a faster quantum tunnelling

relaxation, which is responsible of the low temperature tail. The presence of five crystallographically independent Dy^{3+} ions in the structure with very close DyO_8 coordination environments could be responsible for the existence of different overlapping thermally activated relaxation processes. It is worth noting that even two single-ion relaxation processes have been observed for complexes containing crystallographically equivalent Dy^{3+} sites. At B_{dc} = 0.4 T the QTM is almost suppressed (the tail at low temperature almost disappear) and the high temperature peaks remain roughly at the same temperatures as those observed under zero dc applied field, but exhibiting lower intensity (Figure 12). The fact that magnetic fields as high as 0.4 T are not able to fully eliminate the QTM relaxation process suggests that the remaining QTM process has its origin in hyperfine, and intramolecular and intermolecular magnetic interactions.

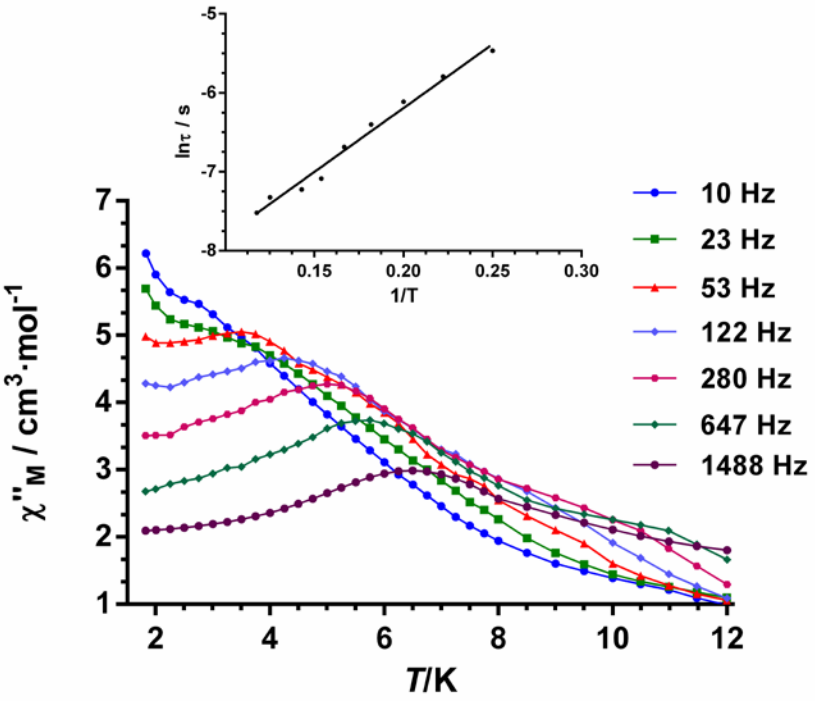

Figure 12. In-phase (χ'_M) and out-of-phase (χ''_M) signals under 0.4 T *dc* field and Arrhenius plot (inset) for **1**.

The Cole-Cole diagram in the temperature range 4.8K (Figure S10) exhibits semicircular shapes that can be fitted using the generalized Debye model, affording α values in the range 0.55-0.64, which supports the existence of a broad distribution of relaxation times. The fit the frequency dependence of χ''_M at each temperature to the generalized Debye model, allowed to extract the relaxation time τ at different temperatures. The results were then used in constructing the Arrhenius plot shown in Figure 12. The linear fit of the data (τ vs 1/T) afforded an effective energy barrier for the reversal of the magnetization of 16.12(8) K with τ_o = 3.3 x 10^{-5} s. The τ_o value is still larger than that usually observed for pure thermally activated processes (typical values are found in the 10^{-7}-10^{-10} s range), thus supporting that the QTM has not been fully suppressed after the application of a *dc* field of 0.4 T, which could be due to hyperfine and intermolecular interactions. It is worth mentioning that the extracted to value for **1** is similar to the values previously reported for a large number of Dy clusters in the same temperature range[18]

The fast relaxation of the magnetization observed for compounds **1** and **6** even in the presence of applied magnetic field could be due to quantum tunneling leading to apparently lower U_{eff} values. It has been recently proposed from theoretical and experimental studies on a dinuclear Dy_2 complex[19] that Dy···Dy intramolecular magnetic exchange interactions in polymetallic Dy^{3+} complexes have the effect of quenching the SMM behavior when the anisotropic axis of the Dy^{3+} ions are not parallel. In complex **1** with a Dy10 wheel structure, as well as in compound **6** whose structure is made of two vertex-sharing Dy_3 triangles turned away from each other, in principle, the principal anisotropic axes could not be parallel and therefore the Ln···Ln interactions could reduce the barrier to magnetization reversal.

Although the Dy^{III} ions in **1** are not strictly in the same plane (they are located

alternatively 0.57 Å above and below the plane), the structure is centrosymmetric and, therefore, the anisotropic axes on opposite Dy centers, if exist, would de parallel but having opposite senses. This together with the antiferromagnetic interaction between the Dy^{III} ions might generate a net quasi-toroidal moment for the projections of the local magnetic moments on to the plane of the wheel. *Ab initio* calculations are planned for the near future.to know whether or not compound **1** is a SMT.

Conclusion

The present work describes the synthesis, structures and magnetic properties of decanuclear Ln_{10} as well as pentanuclear Ln_5 complexes by using a multisite coordination ligand (LH_3). The formation of Ln_{10} and Ln_5 complexes are fully governed by the stoichimetry of the regents used. The dynamic magnetic studies for complex **1** show the SMM behavior with the following characteristics: U_{eff} = 16.12(8) K and τ_o = 3.3 x 10^{-5} s under 0.4 T *dc* field. However, complex **6** shows the frequency dependent maxima in the out-of-phase signal under zero *dc* field, without achieving maxima above 2K. Complexes **3** and **4** show a significant magnetocaloric effect with the following characteristic values: $-\Delta S_m$ = 26.6 J kg^{-1} K^{-1} at T =2.2 K for **3** and $-\Delta S_m$ = 27.1 J kg^{-1} K^{-1} at T = 2.4 K for **4**, both for an applied field change of 7 T.

Experimental Section

Reagents and General Procedures. Solvents and other general reagents used in this work were purified according to standard procedures.[20] 2, 6-Bis(hydroxymethyl)-4-methylphenol, activated manganese (IV) dioxide (MnO_2), $DyCl_3 \cdot 6H_2O$, $TbCl_3 \cdot 6H_2O$, $HoCl_3$. $6H_2O$ and $GdCl_3 \cdot 6H_2O$ were obtained from Sigma Aldrich Chemical Co. and were used as received. 2-Amino ethanol and sodium sulphate (anhydrous) were obtained from S.D. Fine Chemicals, Mumbai, India and

were used as such. 2-(Hydroxymethyl)-6-carbaldehyde-4-methylphenol was prepared according to a literature procedure.[11a]

Instrumentation. Melting points were measured using a JSGW melting point apparatus and are uncorrected. IR spectra were recorded as KBr pellets on a Bruker Vector 22 FT IR spectrophotometer operating at 400-4000 cm^{-1}. Elemental analyses of the compounds were obtained from Thermoquest CE instruments CHNS-O, EA/110 model.

Magnetic Measurements. Field dependence of the magnetization at different temperatures and variable temperature (2−300 K) magnetic susceptibility measurements on polycrystalline samples were carried out with a Quantum Design SQUID MPMS XL-5 device operating at different magnetic fields. Alternating current (ac) susceptibility measurements were performed using an oscillating ac field of 3.5 Oe and ac frequencies ranging from 1 to 1500 Hz. The experimental susceptibilities were corrected for the sample holder and diamagnetism of the constituent atoms by using Pascal's tables. A pellet of the sample cut into very small pieces was placed in the sample holder to prevent any torquing of the microcrystals.

Heat Capacity Measurements. The heat capacity measurements for **3** and **4** were carried out for temperatures down to 0.3 K by using a Quantum Design 9T-PPMS, equipped with a ^{3}He cryostat. The experiments were performed on thin pressed pellets (ca. 1 mg) of a polycrystalline sample, thermalized by ca. 0.2 mg of Apiezon N grease, whose contribution was subtracted by using a phenomenonological expression.

X-ray Crystallography. Single crystals of **1**-**6** were coated with light hydrocarbon oil and mounted in the 100 K dinitrogen stream of a Bruker SMART APEX CCD diffractometer equipped with a CRYO Industries low-temperature apparatus and intensity data were collected using graphite-monochromated Mo Kα radiation (λ = 0.71073 Å). The program SMART[21a] was

used for collecting frames of data, indexing reflections, and determining lattice parameters, SAINT[21a] for integration of the intensity of reflections and scaling, SADABS[21b] for absorption correction, and SHELXTL[21c,d] for space group and structure determination and least-squares refinements on F^2. All the structures were solved by direct methods using the program SHELXS-97[21e] and refined by full-matrix least-squares methods against F^2 with SHELXL-97.[21e] Hydrogen atoms were fixed at calculated positions and their positions were refined by a riding model. All non-hydrogen atoms were refined with anisotropic displacement parameters. Non-positive definite atoms present in compound 3 were treated with ISOR restraints and refined using the Olex-2 software.[21f] The crystallographic figures have been generated using Diamond 3.1e software. [21g] The crystal data and the cell parameters for compounds **1-6** are summarized in Tables 3 and 4. CCDC-1401022 (for **1**), CCDC-1401023 (for **2**); CCDC-1401024 (for **3**); CCDC-1401025 (for **4**); CCDC-1401026 (for **5**), CCDC-1401027 (for **6**), contains crystallographic data for this paper. This data can be obtained free of charge from The Cambridge Crystallographic Data Centre via www.ccdc.cam.ac.uk/data_request/cif.

Table 3. Crystal data and structure refinement parameters of **1-3**.

	1	**2**	**3**
Formula	$C_{177}H_{241}Cl_{27}Dy_{10}N_{14}O_{50}$	$C_{176}H_{240}Cl_{24}N_{14}O_{50}Tb_1$	$C_{176}H_{240}Cl_{24}Gd_{10}N_{14}O_{53}$
M/g	5946.99	5791.82	5823.11
Crystal system	Triclinic	Triclinic	Triclinic
Space group	*P*-1	*P*-1	*P*-1
a/Å	22.0177(11)	22.0256(15)	22.112(2)
b/Å	23.0226(11)	23.0524(15)	23.103(2)
c/Å	24.8075(12)	24.7831(17)	24.886(2)
α(°)	63.2250(10)	63.3580(10)	63.227(2)
β(°)	83.5980(10)	83.503(2)	83.387(2)
γ(°)	82.6300(10)	82.659(2)	82.508(2)
V/Å^3	11113.5(9)	11133.1(13)	11230.6(19)
Z	2	2	2
ρ_c/g cm^{-3}	1.777	1.728	1.722
μ/mm^{-1}	3.714	3.491	3.267

F(000)	5840	5704	5732
Cryst size (mm^3)	0.067 x 0.043 x 0.033	0.035 x 0.021 x 0.016	0.035 x 0.026 x 0.016
θ range (deg)	2.00 to 25.50	4.08 to 25.03	4.09 to 19.55
Limiting indices	-26<=h<=24 -27<=k<=27 -30<=l<=29	-26<=h<=25 -25<=k<=27 -29<=l<=29	-20<=h<=20 -21<=k<=18 -23<=l<=22
Reflns collected	80704	74945	40633
Independent reflns	41251[R(int)=0.0326]	38974 [R(int) =0.0572]	19255 [R_{int} = 0.0581, R_{sigma} = 0.0799]
Completeness to θ(%)	99.7	99.1	98.8
Refinement method	Full-matrix-block least-squares on F^2	Full-matrix-block least-squares on F^2	Full-matrix-block least-squares on F^2
Data/restraints/ parameters	41251 / 44 / 2575	38974 / 46 / 2526	19255/606/2556
Goodness-of-fit on F^2	1.016	1.025	1.044
Final R indices [$I > 2\theta(I)$]	R_1 = 0.0368 wR_2 = 0.0832	R_1 = 0.0576 wR_2 = 0.1360	R_1 = 0.0590 wR_2 = 0.1591
R indices (all data)	R_1 = 0.0572 wR_2 = 0.0914	R_1 = 0.0904 wR_2 = 0.153	R_1 = 0.0742 wR_2 = 0.1719
Largest diff. peak and hole(e ·$Å^{-3}$)	3.602 and -1.606	4.830 and -1.694	4.22 and -1.32

Table 4. Crystal data and structure refinement parameters of **4-6.**

	4	**5**	**6**
Formula	$C_{81}H_{129}Gd_5N_4O_{31}$	$C_{79}H_{123}N_4O_{30}Tb_5$	$C_{81}H_{127}Dy_5N_4O_{30}$
M/g	2441.13	2403.41	2449.37
Crystal system	Monoclinic	Monoclinic	Monoclinic
Space group	$P2_1$	$P2_1$	$P2_1$
a/Å	14.419(5)	14.282(5)	14.445(5)
b/Å	23.412(5)	22.202(5)	23.212(5)
c/Å	16.087(5)	15.875(5)	15.963(5)
β (°)	115.287(5)	110.874(5)	114.046(5)
V/$Å^3$	4910(3)	4703(2)	4888(3)
Z	2	2	2
ρ_c/g cm^{-3}	1.651	1.697	1.664
μ/mm^{-1}	3.405	3.786	3.849
F(000)	2422	2380	2422
Crystal size (mm^3)	0.044 x 0.021 x 0.015	0.062 x 0.037 x 0.024	0.058 x 0.038 x 0.021
θ range (deg)	4.12 to 25.03	4.11 to 25.03	4.10 to 25.03
Limiting indices	-17<=h<=17 -27<=k<=27 -19<=l<=16	-17<=h<=14 -26<=k<=26 -14<=l<=18	-17<=h<=11 -27<=k<=27 -17<=l<=19

Reflns collected	33772	31225	32535
Independent reflns	17214 [*R*(int) = 0.0478]	15993 [*R*(int) = 0.0368]	16934 [*R*(int) = 0.0449]
Completeness to θ (%)	99.5	99.5	99.4
Refinement method	Full-matrix least-squares on F^2	Full-matrix least-squares on F^2	Full-matrix least-squares on F^2
Data/restraints/params	17214 / 30 / 1094	15993 / 15 / 1044	16934 / 12 / 1113
Goodness-of-fit on F^2	1.034	1.029	1.019
Final R indices [$I > 2\theta(I)$]	R_1 = 0.0508 wR_2 = 0.1098	R_1 = 0.0394 wR_2 = 0.0834	R_1 = 0.0435 wR_2 = 0.1053
R indices (all data)	R_1 = 0.0672 wR_2 = 0.1160	R_1 = 0.0502 wR_2 = 0.0873	R_1 = 0.0524 wR_2 = 0.1096
Largest diff. peak and hole(e ·Å^{-3})	1.536 and -1.302	2.250 and -1.451	1.724 and -1.070
Flack parameter	0.010(13)	-0.003(10)	0.013(11)

Synthesis

(*E*)-2-((2-hydroxyethylimino)methyl)-6-(hydroxymethyl)-4-methylphenol (LH_3)

To a stirred solution of **C2** (1.01 g, 6.07 mmol) in dry methanol (20 mL), 2-amino ethanol (0.37 g, 6.07 mmol) also dissolved in dry methanol (10 mL) was added drop wise over a period of 10 min, and the resulting reaction mixture was heated under reflux for 4 h. Then, the reaction mixture was cooled to room temperature. Thereafter the solvent was concentrated in vacuum to 10 mL and kept in a refrigerator at 0 °C for 2 hours to get a bright-yellow crystalline solid which was further suction-filtered, washed with a small amount of cold methanol and air-dried. Yield: 1.06 g, 83.5%. Mp: 95 °C. FT-IR (KBr) cm^{-1}: 3309 (b), 2975 (m), 2865 (m), 1635 (s), 1460 (s), 1360 (w), 1264 (s), 1090 (w), 1074 (s), 971 (w), 864 (s). ^{1}H NMR ($CDCl_3$, δ, ppm): 8.51 (s, 1H, imino), 7.59 (s, 1H, Ar−H), 7.24 (s, 1H, Ar−H), 4.71 (s, 2H, CH_2OH), 3.90 (t, 2H, CH_2), 2.85 (t, 2H, CH_2), 1.29 (s, 3H, CH_3). Anal. Calcd for $C_{11}H_{15}NO_3$ (209.2417): C, 63.14; H, 7.23; N, 6.69 Found: C, 63.21; H, 7.28; N, 6.72.

General Synthetic Procedure for the Preparation of the Complexes 1-3

A general procedure was used for the preparation of these complexes (**1-3**). To a solution of LH_3 (0.06 g, 0.28 mmol) in methanol (5 mL) $LnCl_3 \cdot 6H_2O$ (0.28 mmol) was added and the reaction mixture was stirred at room temperature for 5 minutes. Then subsequently triethylamine (0.08 g, 0.84 mmol) and pivalic acid (PivH) (0.03 g, 0.28 mmol) was added drop wise to this stirring solution. Then the solution was stirred for a further period of 2 h at room temperature to afford a light yellow precipitate which was filtered and washed with cold methanol (2 ml). Then this precipitate re-dissolved in 10 mL of acetonirile/chloroform (1:1) solvent mixture and kept for crystallization in slow evaporation. After about one week, block-shaped, colorless crystals, suitable for X-ray crystallography were obtained. Specific details of each reaction and the characterization data of the products obtained are given below.

$[Dy_{10}(LH)_{10}(\kappa^2\text{-Piv})_{10}] \cdot 9CHCl_3 \cdot 4CH_3CN$ (1)

Quantities: LH_3 (0.06 g, 0.28 mmol), $DyCl_3 \cdot 6H_2O$ (0.10 g, 0.28 mmol), Et_3N (0.08 g, 0.84 mmol), PivH (0.03 g, 0.28 mmol). Yield: 0.078 g, 47 % (based on Dy). Mp: 146 °C (d). IR (KBr) (cm^{-1}): 3120 (b), 2955 (w), 2916 (w), 2828 (w), 1646 (s), 1561 (s), 1541 (s), 1482 (s), 1422 (s), 1361 (s), 1265 (s), 1237 (w), 1174 (w), 1067 (s), 974 (w), 918 (w), 806 (s). Anal. Calcd. for $C_{177}H_{241}Cl_{27}Dy_{10}N_{14}O_{50}$ (5947.07): C, 35.75; H, 4.08; N, 3.30. Found: C, 36.01; H, 4.21; N, 3.35.

$[Tb_{10}(LH)_{10}(\kappa^2\text{-Piv})_{10}] \cdot 8CHCl_3 \cdot 4CH_3CN$ (2)

Quantities: LH_3 (0.06 g, 0.28 mmol), $TbCl_3 \cdot 6H_2O$ (0.10 g, 0.28 mmol), Et_3N (0.08 g, 0.84 mmol), PivH (0.03 g, 0.28 mmol). Yield: 0.082 g, 51 % (based on Tb). Mp: 149 °C (d). IR (KBr) (cm^{-1}): 3125 (b), 2958 (w), 2917 (w), 2826 (w), 1643 (s), 1556 (s), 1541 (s), 1481 (s), 1449 (s), 1363 (s), 1260 (s), 1224 (w), 1174 (w), 1067 (s), 972 (w), 898 (w), 805 (s). Anal. Calcd. for $C_{176}H_{240}Cl_{24}N_{14}O_{50}Tb_{10}$ (5791.96): C, 36.50; H, 4.18; N, 3.39. Found: C, 36.72; H, 4.25; N, 3.40.

$[Gd_{10}(LH)_{10}(\kappa^2\text{-}Piv)_{10}]\cdot 8CHCl_3\cdot 4CH_3CN\cdot 3H_2O$ (3)

Quantities: LH_3 (0.06 g, 0.28 mmol), $GdCl_3\cdot 6H_2O$ (0.10 g, 0.28 mmol), Et_3N (0.08 g, 0.84 mmol), PivH (0.03 g, 0.28 mmol). Yield: 0.043 g, 26 % (based on Gd). Mp: 151 °C (d). IR (KBr) cm^{-1}: 3122 (b), 2960 (w), 2921 (w), 2828 (w), 1643 (s), 1547 (s), 1531 (s), 1485 (s), 1428 (s), 1358 (s), 1263 (s), 1220 (w), 1174 (w), 1087 (s), 972 (w), 897 (w), 803 (s). Anal. Calcd. for $C_{176}H_{240}Cl_{24}Gd_{10}N_{14}O_{53}$ (5823.11): C, 36.3; H, 4.15; N, 3.36. Found: C, 36.01; H, 4.18; N, 3.24.

General Synthetic Procedure for the Preparation of the Complexes 4−6

All the metal complexes (**4−6**) were synthesized according to the following procedure. LH_3 (0.06 g, 0.28 mmol) was dissolved in methanol (10 mL). To this solution $LnCl_3\cdot 6H_2O$ (0.35 mmol) was added and the reaction mixture was stirred at room temperature for 10 minutes. At this stage excess triethylamine (0.14 g, 1.40 mmol) was added drop wise to this solution. Within few minutes the solution was getting turbid. Then, pivalic acid (PivH) (0.057 g, 0.56 mmol) was added to the mixture and was stirred for a further period of 8 h at room temperature to afford a clear yellow solution which was filtered and kept for crystallization in slow evaporation. After about one week, block-shaped, colorless crystals, suitable for X-ray crystallography were obtained. Specific details of each reaction and the characterization data of the products obtained are given below.

$[Gd_5(LH)_4(\mu_2\text{-}\eta^1\eta^1Piv)_4(\eta^1Piv)_3(CH_3OH)]\cdot CH_3OH\cdot 3H_2O$ (4)

Quantities: LH_3 (0.06 g, 0.28 mmol), $GdCl_3\cdot 6H_2O$ (0.13 g, 0.35 mmol), Et_3N (0.14 g, 1.40 mmol), PivH (0.057 g, 0.56 mmol). Yield: 0.095 g, 55.59 % (based on Gd). Mp: 230°C (d). IR (KBr) cm^{-1}: 3397 (b), 2955 (s), 2677 (w), 1648 (s), 1581(s), 1538 (s), 1453 (s), 1374 (s), 1308 (s), 1226 (s), 1178 (w), 1044 (s), 1018 (s), 976 (w), 898 (s), 863 (w). Anal. Calcd. for $C_{81}H_{129}Gd_5N_4O_{31}$ (2441.14): C, 39.85; H, 5.33; N, 2.30. Found: C, 40.03; H, 5.38; N, 2.43.

$[Tb_5(LH)_4(\mu_2\text{-}\eta^1\eta^1Piv)_4(\eta^1Piv)_3(H_2O)]\cdot 3H_2O$ (5)

Quantities: LH_3 (0.06 g, 0.28 mmol), $TbCl_3\cdot 6H_2O$ (0.13 g, 0.35 mmol), Et_3N (0.14 g, 1.40 mmol), PivH (0.057 g, 0.56 mmol). Yield: 0.102 g, 60.62 % (based on Tb). Mp: 230°C (d). IR (KBr) (cm^{-1}): 3390 (b), 2955 (s), 2676 (w), 1649 (s), 1584 (s), 1539 (s), 1454 (s), 1374 (s), 1303 (s), 1227 (s), 1177 (w), 1046 (s), 1018 (s), 977 (w), 897 (s), 863 (w). Anal. Calcd. for $C_{79}H_{123}N_4O_{30}Tb_5$ (2403.47): C, 39.48; H, 5.16; N, 2.33. Found: C, 39.67; H, 5.25; N, 5.41.

$[Dy_5(LH)_4(\mu_2\text{-}\eta^1\eta^1Piv)_4(\eta^1Piv)_3(H_2O)]\cdot CH_3OH\cdot 2H_2O$ (6)

Quantities: LH_3 (0.06 g, 0.28 mmol), $DyCl_3\cdot 6H_2O$ (0.13 g, 0.35 mmol), Et_3N (0.14 g, 1.40 mmol), PivH (0.057 g, 0.56 mmol). Yield: 0.099 g, 57.74 % (based on Dy). Mp: 230°C (d). IR (KBr) (cm^{-1}): 3388 (b), 2956 (s), 2666 (w), 1649 (s), 1586 (s), 1541 (s), 1454 (s), 1360 (s), 1304 (s), 1226 (s), 1178 (w), 1048 (s), 1018 (s), 977 (w), 899 (s), 860 (w). Anal. Calcd. for $C_{81}H_{127}Dy_5N_4O_{30}$ (2449.38): C, 39.72; H, 5.23; N, 2.29. Found: C, 39.79; H, 5.31; N, 2.35.

Acknowledgments

We are thankful to the Department of Science and Technology, New Delhi, for financial support. SD, AD, SK and SB thank CSIR, India for Senior Research Fellowship. VC is thankful to the Department of Science and Technology for a J. C. Bose National Fellowship. EC is thankful for financial support to Ministerio de Economía y Competitividad (MINECO) for Projects CTQ-2011-24478, CTQ2014-56312-P, the Junta de Andalucía (FQM-195 and the Project of excellence P11-FQM-7756), the University of Granada financial support. ME acknowledges financial support from MINECO through grant MAT2012-38318-C03-01. ST thanks the Junta de Andalucía for a postdoctoral contract.

Supporting Information Available

Molecular structures of **2-5**, details structural parameters for the compounds **2-5** and magnetic data. Crystallographic data (excluding structure factors) for the structures in this paper have been deposited with the Cambridge Crystallographic Data Centre as supplementary publication nos. CCDC 1401022-1401027. Copies of the data can be obtained, free of charge, on application to CCDC, 12 Union Road, Cambridge CB2 1EZ, U.K.: http://www.ccdc.cam.ac.uk/cgi-bin/catreq.cgi , e-mail: data_request@ccdc.cam.ac.uk, or fax: +44 1223 336033. This material is available free of charge via the Internet at http://pubs.acs.org.

References

[1] a) G. Christou, D. Gatteschi, D. N. Hendrickson, R. Sessoli, *MRS Bull.* **2000**, *25*, 66–71; b) J. A. Thomas, *Chem. Soc. Rev*. **2007**, *36*, 856-868; c) J. R. Nitschke, *Acc. Chem. Res*. **2007**, *40*, 103-112; d) J. L. C. Rowsell, O. M. Yaghi, *Angew. Chem. Int. Ed*. **2005**, *44*, 4670-4679; e) M. W. Hosseini, *Acc. Chem. Res*. **2005**, *38*, 313-323; f) F. Würthner, C.-C. You, C. R. Saha-Möller, *Chem. Soc. Rev*. **2004**, *33*, 133-146; g) C. N. R. Rao, S. Natarajan, R. Vaidhyanathan, *Angew. Chem. Int. Ed*. **2004**, *43*, 1466-1496.

[2] a) Y. C. Chen, F. S. Guo, Y. Z. Zheng, J. L. Liu, J. D. Leng, R. Tarasenko, M. Orendáč, J. Prokleška, V. Sechovský, M. L. Tong, *Chem. Eur. J.* **2013**, *19*, 14876-14885; b) S. Xue, Y.-N. Guo, L. Zhao, P. Zhang, J. Tang, *Dalton Trans*. **2014**, *43*, 1564-1570; c) F. Gao, L. Cui, Y. Song, Y.-Z. Li, J.-L. Zuo, *Inorg. Chem*. **2014**, *53*, 562-567; e) J. Kan, H. Wang, W. Sun, W. Cao, J. Tao, J. Jiang, *Inorg. Chem*. **2013**, *52*, 8505-8510; f) D. N. Woodruff, R. E. P. Winpenny, R. A. Layfield, *Chem. Rev*. **2013**, *113*, 5110-5148; g) R. J. Blagg, L. Ungur, F. Tuna, J. Speak, P. Comar, D. Collison, W. Wernsdorfer, E. J. L. McInnes, L. F. Chibotaru, R. E. P. Winpenny, *Nat. Chem.* **2013**, *5*, 673-678; h) P. Zhang, Y.-N. Guo, J. Tang, *Coord. Chem. Rev*. **2013**, *257*, 1728-1763; i) F. Habib, M. Murugesu, *Chem. Soc. Rev*. **2013**, *42*, 3278-3288.

[3] a) M. Evangelisti, E. K. Brechin, *Dalton Trans.* **2010**, *39*, 4672; b) J. W. Sharples D. Collison, *Polyhedron* **2013**, *66*, 91-103; d) R. Sessoli, *Angew. Chem., Int. Ed.* **2012**, *51*, 43-45; c) E. Cremades, S. Gómez-Coca, D. Aravena, S. Alvarez, E. Ruiz, *J. Am. Chem. Soc*. **2012**, *134*, 10532; (d) G. Lorusso, M.A. Palacios, G. S. Nichol, E. K. Brechin, O. Roubeau, M. Evangelisti, *Chem. Commun*. **2012**, *48*, 7592; e) G. Lorusso , J. W. Sharples, E. Palacios, O. Roubeau, E. K. Brechin, R. Sessoli, A. Rossin, F. Tuna, E. J. L. McInnes, D. Collison, M. Evangelisti, *Adv. Mater*. **2013**, *25*, 4653; f) F. Luis, M. Evangelisti, *In Molecular Nanomagnet and Related Phenomena*, S. Gao Ed. Springer-Verlag, Berlin-Heidelberg, Germany, **2014**, pp 431-460; g) M. Evangelisti, In Molecular Magnets: Physics and Applications, J. Bartolomé, F. Luis, J. Fernández, Eds, Springer-Verlag, Berlin-Heidelberg, Germany, **2014**, pp 365-385; h) J.-L. Liu, Y.-C. Chen, F.-S. Guo, M-L. Tong, *Coord. Chem. Rev*. **2014**, *281*, 26–49.

[4] a) V. Chandrasekhar, S. Hossain, S. Das, S. Biswas, J. P. Sutter, *Inorg. Chem.* **2013**, *52*, 6346-6353; b) V. Chandrasekhar, S. Das, A. Dey, S. Hossain, J.-P. Sutter, *Inorg. Chem*. **2013**, *52*, 11956-11965; (c) S. Das, S. Hossain, A. Dey, S. Biswas, J.-P. Sutter, V. Chandrasekhar, *Inorg. Chem.* **2014**, *53*, 5020–5028; d) V. Chandrasekhar, P. Bag, E. Colacio, *Inorg. Chem.* **2013**, *52*, 4562-4570.

[5] a) L. G. Westin, M. Kritikos, A. Caneschi, *Chem. Commun*. **2003**, 1012-1013; b) K. H. Zangana, E. M. Pineda, E. J. L. McInnes, J. Schnack, R. E. P. Winpenny, *Chem. Commun*. **2014**, *50*, 1438-1440; c) H. Ke, G.-F. Xu, L. Zhao, J. Tang, X.-Y. Zhang and H.-J. Zhang, *Chem. Eur. J*. **2009**, *15*, 10335-10338.

[6] a) R. J. Blagg, C. A. Muryn, E. J. L. McInnes, F. Tuna, R. E. P. Winpenny, *Angew. Chem. Int. Ed*. **2011**, *50*, 6530-6533; b) M. T. Gamer, Y. Lan, P. W. Roesky, A. K. Powell, R. Cle´rac, *Inorg. Chem*. **2008**, *47*, 6581-6583; c) D. T. Thielemann, A. T. Wagner, Y Lan, C. E. Anson, M.

T. Gamer, A. K. Powell, P. W. Roesky, *Dalton Trans*. **2013**, *42*, 14794-14800; d) J.-B. Peng, X.-J. Kong, Y.-P. Ren, L.-S. Long, R.-B. Huang, L.-S. Zheng, *Inorg. Chem*. **2012**, *51*, 2186-2190; e) H. Tian, L.Zhao, H. Lin, J. Tang, G. Li, *Chem. Eur. J*. **2013**, *19*, 13235-13241.

[7] a) J. Tang, I. Hewitt, N. T. Madhu, G. Chastanet, W. Wernsdorfer, C. E. Anson, C. Benelli, R. Sessoli, A. K. Powell, *Angew. Chem. Int. Ed.* **2006**, *45*, 1729 –1733; b) L. F. Chibotaru, L. Ungur, A. Soncini, *Angew. Chem. Int. Ed*. **2008**, 47, 4126; c) J. Luzon, K. Bernot, I. J. Hewitt, C. E. Anson, A. K. Powell, R. Sessoli, *Phys. Rev. Lett*. **2008**, *100*, 247205; d) I. J. Hewitt, J. Tang, N. T. Madhu, C. E. Anson, Y. Lan, J. Luzon, M. Etienne, R. Sessoli, A. K. Powell, *Angew. Chem. Int. Ed.* **2010**, *49*, 6352-6356.

[8] P.-H. Guo, J.-L. Liu, Z.-M. Zhang, L. Ungur, L. F. Chibotaru, J.- D. Leng, F.-S. Guo, M.-L. Tong, *Inorg. Chem.* **2012**, *51*, 1233-1235.

[9] L. Ungur S. K. Langley, T. N. Hooper, B. Moubaraki, E. K. Brechin, K. S. Murray, L. F. Chibotaru, *J. Am. Chem. Soc*. **2012**, *134*, 18554-18557.

[10] a) G.Novitchi, G. Pilet, L. Ungur, V. V. Moshchalkov, W. Wernsdorfer, L. F. Chibotaru, D. Luneau, A. K. Powell, *Chem. Sci.* **2012**, *3*, 1169-1176; b) S.-Y. Lin, W. Wernsdorfer, L. Ungur, A. K. Powell, Y.-N. Guo, J. Tang, L. Zhao, L. F. Chibotaru, H.-J. Zhang *Angew. Chem. Int. Ed.* **2012**, *51*, 12767 –12771; J. Tang, P. Zhang, in *Lanthanide Single Molecule Magnets*, pp. 127-166, Springer-Verlag Berlin Heidelberg **2015** and references therein; c) L. Ungur S. K. Langley, T. N. Hooper, B. Moubaraki, E. K. Brechin, K. S. Murray, L. F. Chibotaru, *J. Am. Chem. Soc*. **2012**, *134*, 18554-18557.

[11] a) V. Chandrasekhar, S. Das, A. Dey, S. Hossain, F. Lloret, E. Pardo, *Eur. J. Inorg. Chem*. **2013**, 4506-4514; b) S. Das, S. Hossain, A. Dey, S. Biswas, E. Pardo, F. Lloret, V. Chandrasekhar, *Eur. J. Inorg. Chem*. **2014**, 3393-3400; c) V. Chandrasekhar, S. Das, A. Dey, S.

Hossain, S. Kundu, E. Colacio, *Eur. J. Inorg. Chem*. **2014**, 397-406. d) S. Das, A. Dey, S. Kundu, S. Biswas, A. J. Mota, E Colacio, V. Chandrasekhar, *Chem. Asian J.* **2014**, 9, 1876-1887. e) S. Das, K. S. Bejoymohandas, A. Dey, Biswas, M. L. P. Reddy, R. Morales, E. Ruiz, S. Titos-Padilla, E. Colacio, V. Chandrasekhar *Chem. Eur. J*. **2015**, 21, 6449-6464.

[12] a) G. Abbas, Y. Lan, G. E. Kostakis, W. Wernsdorfer, C. E. Anson, A. K. Powell, *Inorg. Chem*. **2010**, *49*, 8067-8072; b) S.-J. Liu, J.-P. Zhao, W.-C. Song, S.-D. Han, Z.-Y. Liu, X.-H. Bu, *Inorg. Chem.* **2013**, *52*, 2103-2109; c) S. K. Langley, N. F. Chilton, I. A. Gass, B. Moubaraki, K. S. Murray, *Dalton Trans*. **2011**, *40*, 12656-12659; d) V. Mereacre, D. Prodius, Y. H. Lan, C. Turta, C. E. Anson, A. K. Powell, *Chem. Eur. J*. **2011**, *17*, 123-128; g) Y. Z. Zheng, M. Evangelisti, R. E. P. Winpenny, *Angew. Chem. Int. Ed*. **2011**, *50*, 3692-3695.

[13] a) J. P. Costes, A. Dupuis, J. P. Laurent, *Inorg. Chim. Acta*. **1998**, *268*, 125-130. b) D. John, W. Urland, *Eur. J. Inorg. Chem.* **2006**, 3503-3509 and references therein. c) F. Avecilla, C. Platas-Iglesias, R. Rodríguez-Cortiñas, G. Guillemot, J. C. G. Bünzli, C. D. Brondino, C. F. G. C. Geraldes, A. de Blas, T. Rodríguez-Blas, *J. Chem. Soc. Dalton Trans*. **2002**, 4658-4665. d) J. Long, F. Habib, P.-H. Lin, I. Korobkov, G. Enright, L. Ungur, W. Wernsdorfer, L. F. Chibotaru, M. Murugesu, *J. Am. Chem. Soc.* **2011**, *133*, 5319-5328. e) L. Cañadillas-Delgado, O. Falbelo, J. Cano, J. Pasán, F. S. Delgado, F. Lloret, M. Julve, C. Ruiz-Pérez, *Cryst.Eng.Commun.* **2009**, *11*, 2131-2142. f) L. E. Roy, T. Hughbanks, *J. Am. Chem. Soc.* **2006**, *128*, 568-575.

[14] F. Chilton, R. P. Anderson, L. D. Turner, A. Soncini, K. S. Murray, *J. Comput. Chem.* **2013**, *34*, 1164-1175.

[15] J.-L. Liu, Y.-C. Chen, F.-S. Guo, M.-L. Tong, *Coord. Chem. Rev*. **2014**, *281*, 26-49.

[16] J. Ruiz, A. J. Mota, A. Rodríguez-Diéguez, S. Titos, J. M. Herrera, E. Ruiz, E. Cremades, J. P. Costes, E. Colacio, *Chem Commun*. **2012**, *48*, 7916-7918 and references therein.

[17] J. D. Rinehart, J. R. Long, *Chem. Sci.* **2011**, *2*, 2078-2085.

[18] a) C. Ritchie, M. Speldrich, R. W. Gable, L. Sorace, P. Kögerler, C. Boskovic, *Inorg. Chem.* **2011**, *50*, 7004-7014; b) K. Katoh, K. Umetsu, B. K. Breedlove, M. Yamashita, *Sci. China Chem.* **2012**, *55*, 918; c) S. Y. Lin, L. Zhao, Y. N. Guo, P. Zhang, Y. Guo, J. Tang, *Inorg. Chem*. **2012**, *51*, 10522-10528; d) S. K. Langley, N. F. Chilton, I. A. Gass, B. Moubaraki, K. S. Murray, *Dalton Trans.* **2011**, *40*, 12656-12659; e) H. Tian, Y. N. Guo, L. Zhao, J. Tang, Z. Liu, *Inorg. Chem*. **2011**, *50*, 8688-8690.

[19] E. Moreno Pineda, N. F. Chilton, R. Marx, M. Dörfel, D. O. Sells, P. Neugebauer, S.-D. Jiang, D. Collison, J. van Slageren, E. J.L. McInnes, R.E.P. Winpenny, *Nat. Commum*. **2014**, *5*, 5243-5250.

[20] B. S. Furniss, A. J. Hannaford, P. W. G. Smith, A. R. Tatchell, *Vogel's Textbook of Practical Organic Chemistry*, 5th ed.; ELBS, Longman: London, **1989**.

[21] a) *SMART & SAINT Software Reference manuals, Version 6.45*, Bruker Analytical X-ray Systems, Inc., Madison, WI, **2003**; b) G. M. Sheldrick, *SADABS, a software for empirical absorption correction, Ver. 2.05*, University of Göttingen, Göttingen, Germany, **2002**; c) *SHELXTL, Reference Manual, Ver. 6.1*, Bruker Analytical X-ray Systems, Inc., Madison, WI, 2000; d) G. M. Sheldrick, *SHELXTL, Ver. 6.12*, Bruker AXS Inc., Madison, WI, **2001**; e) G. M. Sheldrick, *SHELXL97, Program for Crystal Structure Refinement*, University of Göttingen, Göttingen, Germany, **1997**; f) O.V. Dolomanov, L.J. Bourhis, R.J. Gildea, J.A.K. Howard, H. Puschmann, *J.Appl. Cryst.* **2009**, *42*, 339-341; g) K. Bradenburg, *Diamond, Ver. 3.1eM*, Crystal Impact GbR, Bonn, Germany, **2005**.

Graphical Abstract

The sequential reaction of multidentate flexible Schiff base ligand (LH_3), $LnCl_3 \cdot 6H_2O$ and pivalic acid in presence of triethyl amine as a base with stoichiometric ratio 1:1:1:3 and 1:1.25:2:5 afforded series of homometallic decanuclear complexes, $[Ln_{10}(LH)_{10}(\kappa^2\text{-Piv})_{10}]$ (Ln = Dy, Tb and Gd) and homometallic pentanuclear complexes, $[Ln_5(LH)_4(\mu_2\text{-}\eta^1\eta^1\text{Piv})_4(\eta^1\text{Piv})(S)]$ (Ln = Dy, Tb and Gd) respectively. Detailed magnetic analysis of all the complexes concluded the SMM behavior exhibited by Dy^{3+} analogues and Gd^{3+} complexes show significant magnetocaloric effect.